

# ZINC92180466: A Novel Small Molecule ARBF-3 Binder for Non-metastatic CRPC Therapy through *In-silico* Pharmacophore Modeling, Docking, and **Molecular Dynamics Simulations**

\*1Na'Allah, A., 2Maikarfi, M. and 1Alabi, M.A.

<sup>1</sup>Department of Biochemistry, Kwara State University, Malete, Nigeria <sup>2</sup>Department of Biochemistry, Kaduna Polytechnic, Kaduna, Nigeria

#### **Abstract**

Prostate cancer presents a major global health concern despite advancements in prostate-specific antigen testing and treatment resulting in reduced mortality rates. However, metastatic and non-metastatic castrate-resistant prostate cancer (CRPC) persists as a significant challenge. Emerging research suggests targeting the non-ligand-binding (non-LBD) site such as the binding function 3 region (BF3) of the androgen receptor 1 (AR1) protein, as a promising approach to combat progression of the disease. This underscores the necessity for developing novel AR signaling inhibitors. This study aimed to identify a novel small molecule inhibitor for non-metastatic CRPC therapy by targeting the BF-3 region for promising improved patient outcomes. *In-silico* pharmacophore modeling, QSAR analysis, and molecular docking were conducted followed by molecular dynamics simulations and binding free energy calculations. The results of this study highlighted key pharmacophoric features for effective AR1 inhibition, that may serve as a guide for the design of novel inhibitors. ZINC92180466 emerged as a promising AR1 BF3-binding compound, while energy decomposition analysis elucidated crucial ligand-receptor interactions. Overall, the study underscores the potential of AR1-targeted therapies in combating prostate cancer, particularly at non-LBD sites such as the BF3 region, thereby offering avenues for the rapeutic advancement and improved prostate cancer patient prognosis.

Keywords: Androgen receptor, BF-3 region, CRPC, small molecule inhibitors, QSAR analysis

#### 1. Introduction

Prostate cancer (PCa), the most diagnosed cancer in men, remains a significant global health burden due to a rise in prostate cancer incidence [1]. However, there is a decline in mortality rate in developed nations due to early detection, increased prostate-specific antigen (PSA) testing and improved treatment and [2,3]. The primary treatment for metastatic hormone-sensitive prostate cancer involves androgen deprivation therapy (ADT) to suppress testosterone levels. However, a considerable portion of cases usually progress to metastatic castrate-resistant prostate cancer (mCRPC) otherwise known as the terminal phase, thereby highlighting the limitations of traditional hormonal therapies [4-6]. The androgen receptor (AR) plays a critical role in male reproductive functions and is intricately linked to the development and progression of PCa, thereby explaining its critical role in current PCa therapeutic strategies [7,8]. AR signaling represents a critical pathway in prostate cancer, which is evidenced by the initial reliance on androgen-deprivation therapy for patient treatment [9,10], while prostate cancer patients with diminishing responsiveness to such therapy are classified as castration-resistant prostate cancer (CRPC) patients, with continued reliance of the condition on AR signaling process [11,12].

The AR protein, as a member of the nuclear receptor (NR) family, is composed of four key regions, which are a unique N-terminal domain (NTD), a DNA-binding domain (DBD), a brief hinge region, as well as a C-terminal ligand-binding domain (LBD) [13-15]. The binding of testosterone or dihydrotestosterone (DHT) to the ligand binding pocket (LBP) of the AR LBD usually induces a conformational shift in AR, thereby triggering dissociation from heat shock proteins, dimerization, and translocation to the cell nucleus [16,17]. Subsequently, the AR dimer binds to the androgen response element (ARE) on DNA to regulate gene transcription, while the positive linkage between abnormal AR activity and PCa has been scientifically established [18,19].

\*Corresponding Author E-mail address: asiat.naallah@kwasu.edu.ng Received: March 13, 2025; Revised: June 10, 2025;

Accepted and Published: June 23, 2025





Endocrine therapy targeting AR has been a cornerstone in PCa treatment, yet challenges persist due to AR point mutations and increased constitutively active receptor expression [20,21]. Moreso, perturbations in the AR signaling process arising from factors such as androgen synthesis, AR amplification, mutations, or alternative splicing generating AR variants (AR-Vs) have been shown to contribute to resistance mechanisms against current therapies targeting especially the AR LBD [22,23]. Thus, ongoing investigations into the role of AR in advanced PCa have spurred the search for novel AR signaling inhibitors with enhanced efficacy in improving the survival of PCa patients [24,3], as androgen-dependent initiation and PCa progression have long prompted efforts to inhibit the characteristic androgen biosynthesis or AR function in this condition [25,26]. Continued research on the role of androgen receptors in advanced PCa has also fueled the quest for innovative AR signaling inhibitors for PCa patient outcomes optimization [27,28]. Additionally, androgen withdrawal through androgen deprivation therapy (ADT) or direct AR targeting via anti-androgens reduces AR activity, leading to cancer cell cycle arrest, apoptosis induction, as well as tumour volume reduction [29,30]. This is because androgen receptor antagonists or anti-androgens play a critical role in the suppression of AR signaling by binding to the LBD, thereby disrupting androgen-induced activation and observable shift towards proliferation during cancer progression and uncontrolled growth of dysregulated androgen-induced castration-resistant prostate cancer condition [31,32].

Most conventional approaches focused on the inhibition of nuclear receptor activity by targeting the hormone-binding pocket which results in a significantly improved survival rate of prostate cancer patients [33,34]. However, they have been associated with diverse potency limitations due to the heterogeneity of prostate cancer conditions as well as diverse safety limitations of the inhibitory agents [35,36]. An alternative approach involving inhibitors binding to AR surfaces to facilitate the assembly of receptor-binding partners for overcoming these constraints has been suggested [37]. The study identified potent inhibitors binding to a regulatory surface cleft termed binding function (BF)-3, a known target for mutations in PCa and a promising pharmaceutical target for novel therapeutic interventions, thereby offering the potential to extend the survival of patients as well as prevent the shift towards poor prognosis-liable therapeutic resistance mechanisms. Therefore, the aim of the present study was to identify a novel effective, and clinically safe small molecule inhibitor of androgen receptor binding function-3 pocket (BF-3) as a therapeutic target for non-metastatic castration-resistant prostate cancer (CRPC).

#### 2. Materials and Methods

#### 2.1 Ligand-Based Pharmacophore Modeling of Standard Androgen Receptor 1 Inhibitors

Structure-based pharmacophore modeling was carried out according to standard method [38]. Briefly, five randomly selected AR1 inhibitors with experimentally validated activity were retrieved from ChEMBL database to ensure diversity in chemical structures and inhibitory potencies. The dataset underwent meticulous curation involving removal of duplicates, standardization of chemical structures, and annotation of biological activities. This step is crucial for ensuring the quality and reliability of the dataset used for pharmacophore modeling. Conformational sampling was then performed on each inhibitor molecule in the dataset to generate multiple low-energy conformations using the Schrödinger Maestro. The conformations that represent energetically favourable and diverse molecular geometries were retained for further analysis. The pharmacophoric features shared among the AR1 inhibitors were identified including hydrogen bond donors, acceptors, aromatic rings, and hydrophobic groups. The conformations of the inhibitors were aligned based on these pharmacophoric features using alignment algorithms with a focus on maximizing feature overlap to ensure that the essential structural motifs contributing to AR1 inhibition are appropriately superimposed with minimal structural deviations.

The pharmacophore hypotheses were then generated using the Schrödinger Phase and subjected to rigorous validation to assess their predictive accuracy and robustness using Fischer's randomization test. The decoy set validation was done to evaluate the performance of the pharmacophore model before it was applied for virtual screening of the ZINC database to identify potential AR1 inhibitors. The model was interpreted to understand the structural requirements for AR1 inhibition as a guide for the design of novel inhibitors. The results of the pharmacophore modeling including generated hypotheses, validation metrics, visual representations of pharmacophore features and spatial arrangements were documented for better understanding and reproducibility. This was then used to filter the ZINC database using the X: 21.22, Y: 32.04, Z: 42.08 coordinates at the ligand features of hydrophobicity, aromatic rings, hydrogen bond donor, hydrogen bond acceptor, as well as the exclusion sphere, through the ZINC pharmer (http://zincpharmer.csb.pitt.edu/pharmer.html) which yielded 32, 947 compounds.



# Int. J. Biomed. Health Sci. 2025; 19(1): 61-85

#### 2.2 Collection and Pre-processing of data for QSAR Analysis of AR1 Compounds

A dataset comprising 400 chemical compounds known to inhibit AR1 protein was retrieved from the ChEMBL database to ensure dataset reliability and diversity. The dataset was then pre-processed by filtering out irrelevant compounds, eliminating duplicates, and standardizing chemical representations to maintain uniformity and consistency in the dataset in readiness for QSAR analysis.

#### 2.3 Descriptor Calculation and Development of Model for QSAR Analysis

The 1D and 2D molecular descriptors of each compound were computed using the Padel software. These calculated essential features of the compounds help to facilitate subsequent modeling processes and offer quantitative representations of various physicochemical properties and structural characteristics. The QSAR models were developed from calculated molecular descriptors by using the standalone Drug Theoretics and Chemoinformatics Laboratory (DTC lab) tools. The 400 compound datasets were divided according to Kernard-Stone method into training set (70%) and test set (30%) for the development of genetic algorithm-multiple linear regression (GA-MLR) model. This was following data pre-treatment at a variance cut-off of 0.001 and inter-R<sup>2</sup> cut-off of 0.99. One hundred (100) iterations were performed at the equation length of 2, and mutation probability of 0.3 at a range of 0 to 1. A total of 100 equations were initially generated out of which five were selected based on mean absolute error (MAE)-based criteria of fitness function.

#### 2.4 Model Evaluation for QSAR Analysis (External Validation)

The trained model was rigorously assessed for their predictive performance and reliability through their R-squared (R²), Root Mean Square Error (RMSE), and Cross-Validation evaluation to gauge the accuracy and generalization capabilities of the model, as well as ensure that the developed model effectively captured the underlying relationships within the dataset. A separate test set of AR1 compounds (30%), distinct from the training dataset, was employed to externally evaluate the predictive performance of the model by using metrics similar to the internal validation phase to ensure the robustness and applicability of the model for unseen data as well as validate extra confidence in the predictive capability of the model.

# 2.5 Standard Precision and Quantum Polarized Ligand Docking of Compounds obtained from Pharmacophore Screening of ZINC Database

#### 2.5.1 Protein Preparation

The crystal structure of human AR1 (PDB ID: 2PIP) was retrieved from the Protein Data Bank website (http://www.rcsb.org). The structure was prepared using protein preparation wizard of Schrodinger Maestro version 12.5.139 which involved removal of co-crystallized compounds, refinement of protein chain using the OPLS2005 force field, and adjustment of pH to 7.0-7.2. Steric clashes were addressed, and hydrogen bond orders were restored using Epik. Also, missing side chains and loops were substituted with appropriate structures by using the Prime module. Additionally, water molecules with a molecular weight exceeding 5.0 and fewer than three hydrogen bonds with non-water entities from the ionized (Het) groups were eliminated, which were then followed by an energetic minimization step with a polarity charge cut off set at 0.25 [39, 40].

#### 2.5.2 Ligand Preparation

The two-dimensional structures of the extracted ZINC compounds and the standard AR1 inhibitor in this study were prepared by using the ligand preparation wizard of Schrodinger Maestro. This involved generating possible Epik states and tautomers of the ligand within a target pH range of 7.0 to 7.2, before subsequent energy minimization of the prepared ligands by using the MacroModel wizard under the OPLS2005 force field.

#### 2.5.3 Receptor Grid Generation

The co-crystallized ligand, which also functioned as the standard inhibitor for the AR1 protein, underwent isolation from the receptor chain's active site. This process was carried out using the designated receptor. To ensure precision, atoms with Van der Waals radii of 1.0 Å and partial atomic charges of less than 0.25 Å were considered according to





the default criterion. Defining the active site involved creating an enclosing box around the selected residues neighbouring the co-crystallized ligands at coordinates (x, y, z = '80', '80', '80'). The workspace centroid then served as the reference point for generating a grid centered on the ligand, following the default Glide settings protocol, and subsequently docking all studied ligands.

#### 2.5.4 Glide Standard Precision Docking

Multiple conformations of each ligand of compounds filtered from the ZINC database (32, 948 compounds) were subjected to docking into the receptor grid using Glide standard precision. This process accounted for factors such as nitrogen inversion and ring conformations. Post-docking minimization was then performed to refine the ligand poses further. The docking score was determined based on the input partial charges. It is important to highlight that ligands containing more than 500 atoms were excluded from both the docking and scoring processes. Moreover, the van der Waals radii of ligand atoms with partial atomic charges were scaled by 0.80 to improve accuracy relative to a partial charge cut off of 0.15. Epik state penalties were also integrated into the docking score calculations [41-43].

#### 2.5.5 Glide Quantum Polarized Ligand Docking

The charges for the ligands during the Glide docking process were initially determined using the standard semiempirical method. This involved eliminating duplicate poses if the root mean square deviation was less than 0.5 Å and the maximum atomic displacement was less than 1.3 Å. Subsequently, quantum mechanics charges were computed for the ligands in their free state within the gas phase before redocking using the Glide extra precision feature. The binding affinity was then calculated using the Coulson charge semi-empirical method. The ligands with the most favorable binding poses were selected based on their Glide Score. It is noteworthy that for the receptor, the van der Waals scaling factor was set to 1.0, while for the ligand, it was set to 0.8 to optimize the interactions [44,45].

#### 2.5.6 Molecular Mechanics-Generalized Born Surface Area Calculations

Schrodinger Maestro Prime was employed to calculate the molecular mechanics generalized Born surface area free energy change (MMGBSA dG) for the docked ligands. The method utilized variable dielectric generalized-Born (VSGB) solvation model and the provided ligand partial charges, while the target flexible residues were constrained throughout these calculations [46,47].

#### 2.5.7 Protein-Ligand Interaction Analysis

The Glide merging procedure was employed to create complexes of docked ligands at their optimal binding poses with the protein before visualizing two-dimensional interactions between these ligands and the residues within the binding pocket of the target using the BIOVIA Discovery Studio suite. Additionally, Schrodinger PyMol® was utilized for a more detailed representation of interactions of the docked compounds with the target active pocket.

#### 2.6 Molecular Dynamic (MD) Simulation

The complexes from docking analysis of the two top docked compounds and the unbound proteins were further subjected to full 50 ns atomistic molecular dynamics. For the docking process, previously reported standard techniques were employed [48-50]. The CHARMM36m force field was used to determine the parameters for ions, water molecules, and amino acids in proteins. Conversely, small molecules were parameterized using the CHARMM general force field (CGenFF) tool, which is part of CHARMM-GUI [51-53] GROMACS 2020.3 was employed for simulation [54]. Using the TIP3P water model with a 1 nm padding, the systems were solvated in a cubic box. NaCl ions were then added to the system at a concentration of 0.154 M. An MD package was used to carry out the simulation, applying periodic boundary conditions (PBC) in three directions. Initially, the maximum permitted force of 100 KJ.mol-¹nm⁻¹ and the number of steps set to 100,000 minimization steps were utilised to minimize the system's potential energy and remove atomic collisions using the steepest descent technique. We began with an NVT ensemble, in which the volume, temperature, and number of atoms were held constant. Subsequently, the V-rescale approach was used to equilibrate the temperature to 310 K, while maintaining an atmospheric pressure of one using a Berendsen barostat [55]. Lastly, an NVT ensemble production run lasting 100 ns was executed. The hydrogen-bonded atoms' bond lengths were limited in every step by the LINear Constraint Solver (LINCS) algorithm [56].





The Particle Mesh Ewald (PME) technique was utilized to calculate electrostatics, with a 1.2 nm cutoff. Using a leap-frog approach, the Newtonian equations of motion were integrated, with a time step of 1 femtosecond for the equilibration stages and 2 femtoseconds for the production steps. Every 0.1 ns of the production run a frame was recorded, summing to 1000 frames per system. A frame was recorded every 0.1 second during the production cycle, for a total of 1000 frames per system [57]. The Root means square deviation (RMSD) for the protein alone, the ligand alone, and the protein-ligand complex, root mean square fluctuation (RMSF) of  $C_{\alpha}$  atoms, solvent accessible surface area (SASA), radius of gyration (RoG), number of hydrogen bonds, and separation of center of mass of ligand and protein were all computed.

#### 2.7 Binding Free Energy Calculation Using Molecular Mechanics Generalised Born Surface Area

Using the Molecular Mechanics Generalised Born Surface Area (MM-GBSA) method and decomposition analysis to obtain the binding energies of amino acids within 0.5 nm of the ligand using the gmx MMPBSA package, the binding free energy of the two top docked phytochemicals from the initial docking analysis were further determined. The methods used were the same as those initially published [58-60].

#### 2.8 Clustering of Molecular Dynamic Trajectories of Unbound Proteins

The molecular trajectories of the complexes after 100 ns MDS were subjected to cluster analysis using Trusty Trajectory Clustering (TTClust) V 4.9.0 [58]. The systems were clustered automatically utilizing TTClust python package, which utilizes the elbow method to determine the optimal number of clusters and finally produce a representative frame for each cluster. A representative confirmation from each cluster was selected. The analysis of each cluster was based on RMSD values, concerning the starting geometry and the minimum energy conformation of the most populated cluster was taken as the most reliable solution.

#### 3. Results and Discussion

#### 3.1 Ligand-based Pharmacophore Modelling

One of the significant findings of this study is the identification of common pharmacophoric features among the AR1 inhibitors, including hydrogen bond donors, hydrogen bond acceptors, aromatic rings, and hydrophobic groups (Figure 1). These features exhibited relatively positive HypoScores (Figure 2) and are essential for establishing favourable interactions with the AR1 binding pocket, to facilitate ligand-receptor recognition and binding. The spatial arrangement and distribution of these pharmacophoric features in the chemical structures of the inhibitors highlight the critical regions responsible for their inhibitory potency. Furthermore, the ligand-based pharmacophore model generated consensus pharmacophore hypotheses that represent the optimal arrangement of pharmacophoric features for AR1 inhibition (Figure 3). These hypotheses provide a structural framework for the rational design of novel AR1 inhibitors with enhanced potency and selectivity. Thus, by aligning the inhibitors based on their pharmacophore features, chemical modifications, and substitutions that are likely to improve ligand binding affinity and therapeutic efficacy can always be prioritized in the drug development process.

The results obtained from the comprehensive ligand-based pharmacophore modeling of five AR1 inhibitors in this study provide valuable insights into the structural requirements for effective AR1 inhibition. Through analysis of chemical features of the inhibitors and their shared pharmacophoric features, key molecular determinants essential for ligand binding and modulation of AR1 activity have been identified. Therefore, the insights gained from this study have implications for developing therapeutics targeting prostate cancer by understanding the structural requirements influencing the AR1 activity. This can help expedite the discovery and optimization of novel inhibitors of AR1, thereby ultimately leading to the development of more effective treatments for this pathological condition. Overall, the comprehensive ligand-based pharmacophore modeling results provide a roadmap for the rational design and optimization of AR1 inhibitors, which offers new opportunities for drug discovery and development in the field of androgen receptor modulation. Thus, by leveraging these insights, the discovery and development of therapeutic agents for conditions such as prostate cancer, androgenetic alopecia, and other androgen-related diseases can be expedited.



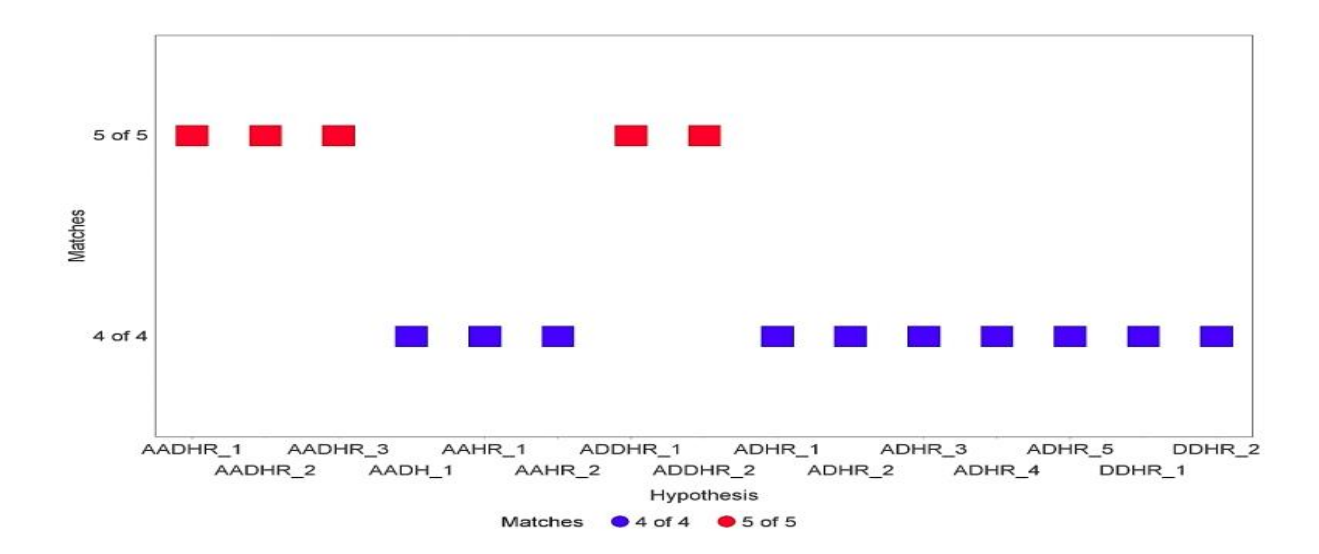


Figure 1: Enrichment Report for the Top Best Five Pharmacophore Hypothesis

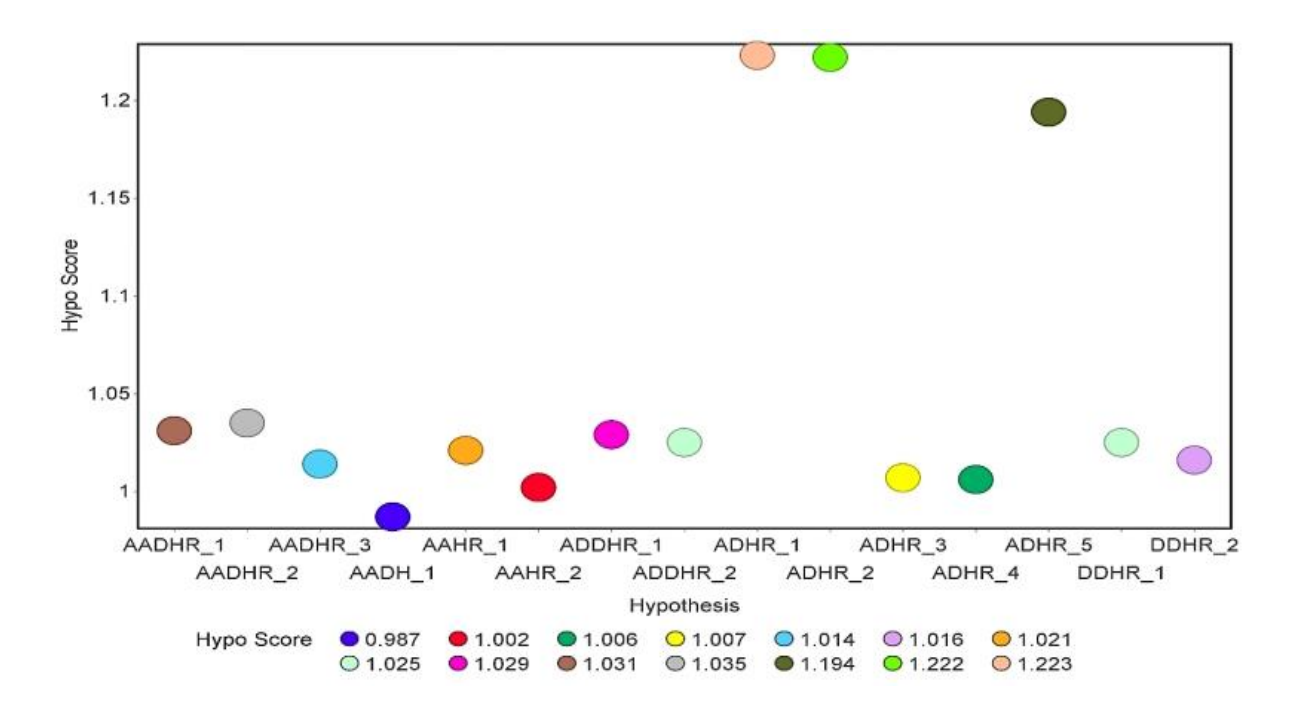


Figure 2: HypoScore Values of Top Best Five Pharmacophore Hypothesis



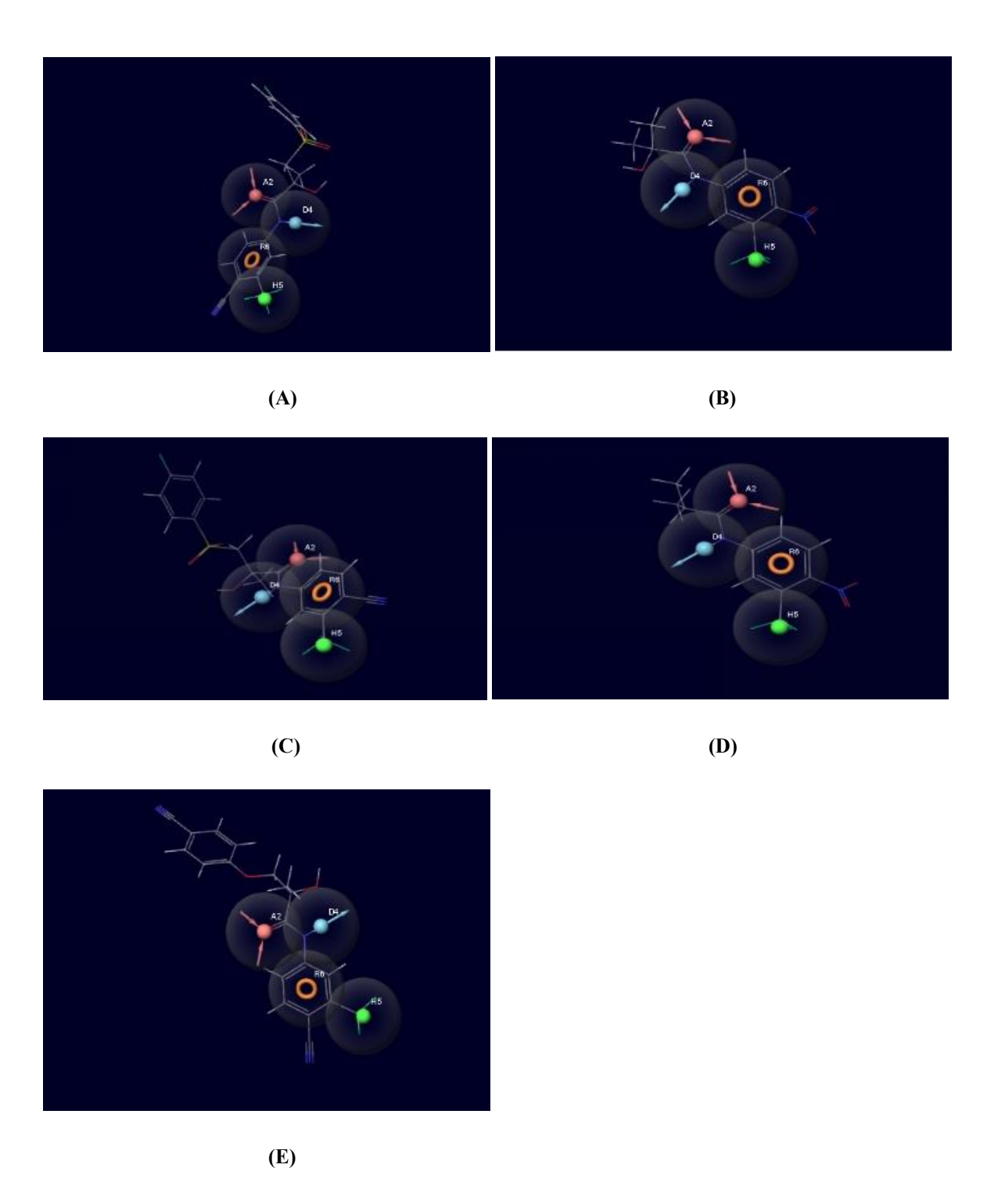


Figure 3: Top Best Five Pharmacophore Hypothesis from the AR1 Inhibitors in the Order of (A), (B), (C), (D), and (E) with the Highest Inhibitory Activity. Key: (A) ADHR\_1 (B) ADHR\_2 (C) ADHR\_5 (D) AADHR\_2 (E) AADHR\_1 Where A: Hydrogen bond acceptor; D: Hydrogen bond donor; R: Alkyl group



# 3.2 Decoy Set Validation of Pharmacophore Hypothesis

The decoy compounds screened against the pharmacophore model showed low activity predictions (Figure 4), thereby indicating the high specificity of the model and minimal false positives. The receiver operating characteristic curve analysis is a measure of the sensitivity and specificity of the pharmacophore model, with true positive rate (sensitivity) and false positive rate (1-specificity) being calculated at different activity thresholds. The area under the curve (AUC) is a measure of the model performance, with higher AUC values indicating better predictive power. In this study, a value of 0.8 was recorded which suggests good discriminatory power of the pharmacophore model between the active and inactive compounds. The validation tests show the reliability, robustness, and predictive accuracy of the ligand-based pharmacophore model for AR1 inhibitors, which supports its use in virtual screening and compound design. Thus, using a decoy set of compounds with similar properties but different activities helped assess the specificity of the model, while screening these decoy compounds revealed low activity predictions, thereby indicating high specificity and minimal false positives. Additionally, the receiver operating characteristic (ROC) curve analysis (Figure 5) confirmed the sensitivity and specificity of the model, with an AUC value of 0.8 indicating strong discriminatory power between the active and inactive compounds. These results further affirm the reliability and applicability of the model in accurately predicting AR1 inhibitor activity, promising potential in drug discovery for relevant diseases.

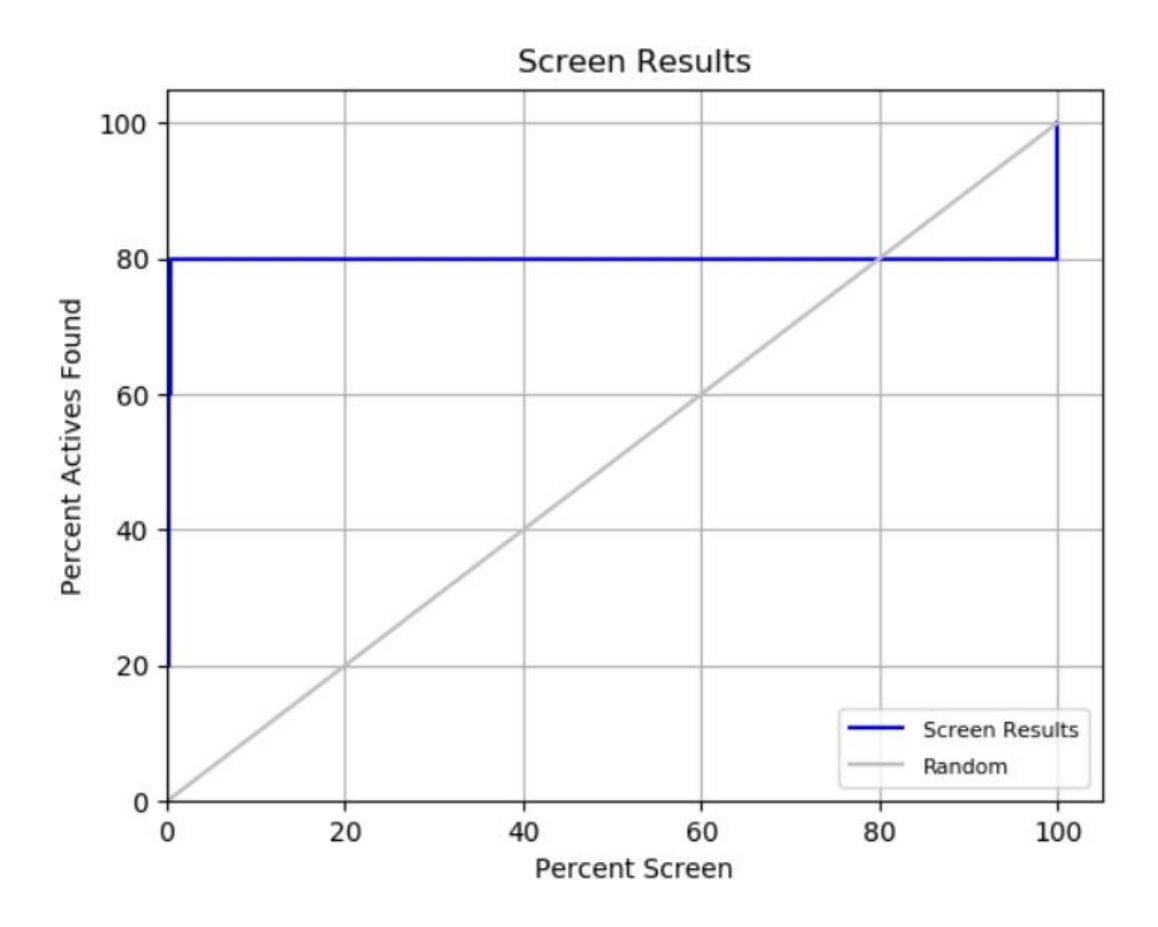


Figure 4: Screen Results of Decoy Set Validation of the AR 1 Inhibitors Pharmacophore Model



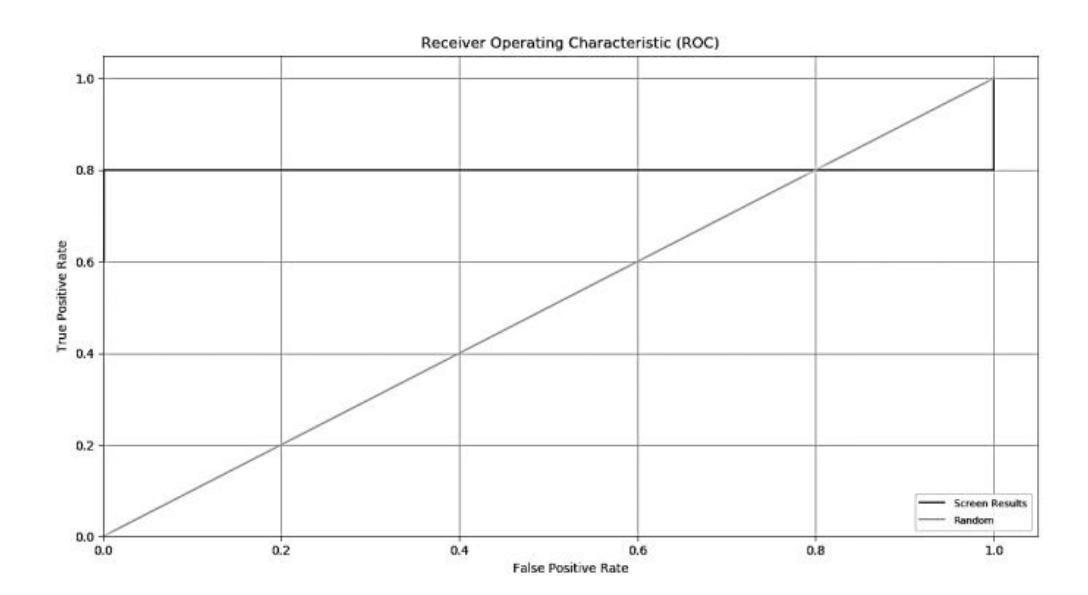


Figure 5: Receiver Operating Characteristics of Decoy Set Validation of the Model

#### 3.3 Two-Dimensional Quantitative Structure-Activity Relationship (OSAR) Model Result

The fitness score of the Genetic Algorithm-Multiple Linear Regression (GA-MLR) model, assessed using MAE-based criteria, is 1.4658. This score indicates the overall quality of the model in predicting the activity of AR1 inhibitors, with lower values indicating better predictive performance (Figure 6). The Multiple Linear Regression (MLR) equation derived from the GA-MLR model is expressed as PIC50 = -69.2105 (+/-2.8837) + 2.6808 (+/-0.0438) nBondsS3 + 0.1137 (+/-0.0056) TopoPSA + 122.0269 (+/-4.8235) AVP-0. This equation represents the relationship between the predictor variables (nBondsS3, TopoPSA, AVP-0) and the response variable (PIC50), which is a measure of the compound's potency in inhibiting AR1 activity. The coefficients associated with each predictor variable indicate the magnitude and direction of their influence on the predicted PIC50 values. Furthermore, the model was trained using a dataset comprising 280 data points, indicating the number of compounds for which both predictor variables and corresponding experimental PIC50 values were available. Additionally, the model selected three features (nBondsS3, TopoPSA, AVP-0) as relevant descriptors for predicting AR1 inhibition activity, suggesting that these molecular features play a crucial role in determining the potency of AR1 inhibitors.

The GA-MLR model provides valuable insights into the SAR of AR1 inhibitors, facilitating the identification and design of novel compounds with improved potency against AR1 for potential therapeutic applications. The comprehensive QSAR analysis conducted on a dataset comprising 400 compounds targeting the androgen receptor 1 (AR1) extracted from the ChEMBL database holds significant promise for the discovery of novel inhibitors specifically tailored for the treatment of non-metastatic castration-resistant prostate cancer (CRPC). Given the critical role of AR1 signaling in prostate cancer progression, especially in the castration-resistant stage where standard androgen deprivation therapy loses efficacy, the development of potent and selective AR1 inhibitors is of paramount importance. The robustness of the QSAR model, as indicated by high internal validation metrics such as R^2, adjusted R^2, and Q^2(LOO), underscores its reliability in predicting the inhibitory potency of compounds against AR1. These metrics assure confidence in the model's ability to accurately discern structural features associated with AR1 inhibition, facilitating the identification of lead compounds with enhanced activity against the target.



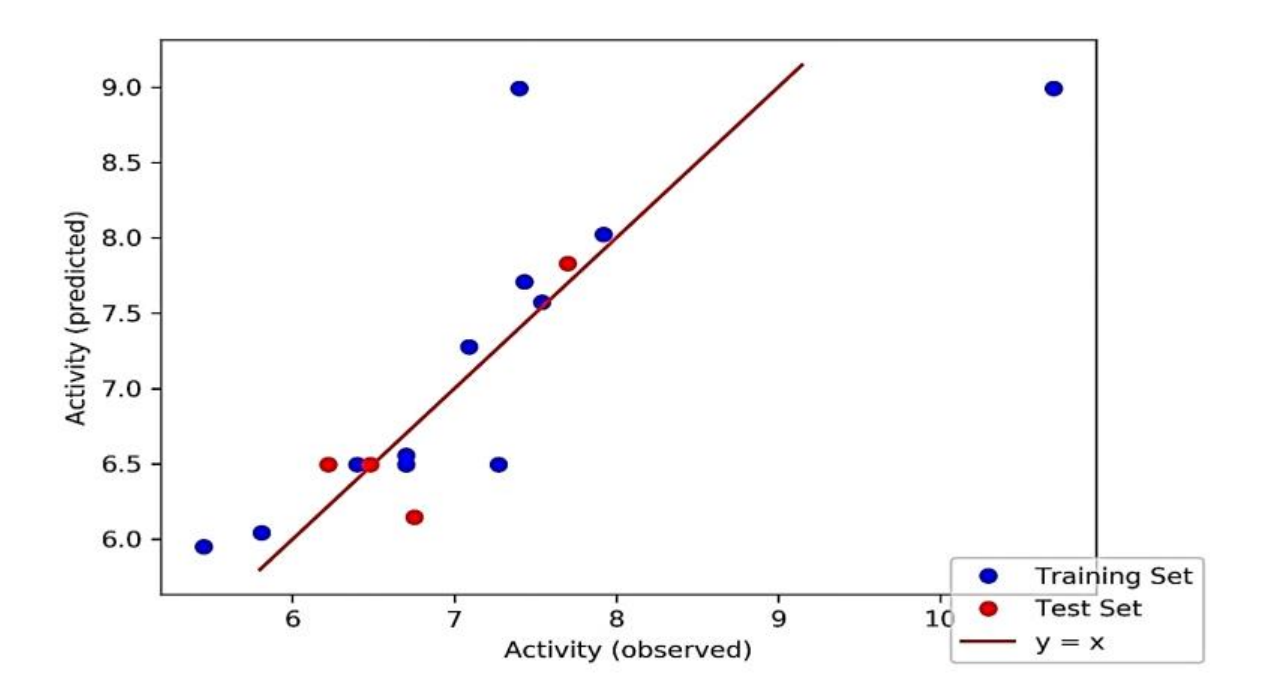


Figure 6: Best Model Genetic Algorithm-Multiple Linear Regression of Quantitative Structure-Activity Relationship Between the First 15 Data Points (Test and Training Datasets) of AR 1 Inhibitors

External validation of the QSAR model further reinforces its utility in virtual screening efforts aimed at discovering novel AR1 inhibitors for CRPC therapy. The high Q^2(F1) test and Q^2(F2) test values, along with the coefficient of determination and mean absolute error (MAE) for the test set, signify the model's consistency and accuracy in predicting the activity of unseen compounds. This reliability is crucial for prioritizing compounds with the greatest likelihood of efficacy in preclinical and clinical settings. Additionally, the MAE-based prediction quality of the model, deemed "GOOD" for both internal and external validation, further assures its suitability for identifying potential drug candidates with favourable pharmacological profiles. The implications of the QSAR findings extend beyond predictive modeling, which offers valuable insights into the structural determinants of AR1 inhibition. The QSAR model, by elucidating the key molecular features associated with enhanced inhibitory activity, helps to facilitate rational drug design strategies that are aimed at optimizing the potency, selectivity, and pharmacokinetic properties of AR1 inhibitors. This knowledge-driven approach is particularly relevant in the context of CRPC therapy, where the development of novel therapeutics capable of overcoming resistance mechanisms and improving patient outcomes remains a significant unmet need. Therefore, the comprehensive QSAR analysis of AR1 inhibitors represents a critical step forward in the quest for innovative therapies for CRPC, which can expedite the discovery and optimization of lead compounds with the potential to disrupt AR1 signaling pathways and impede prostate cancer progression by leveraging computational modeling techniques to interrogate large chemical datasets. Ultimately, these efforts hold promise for advancing precision medicine approaches tailored to the unique molecular characteristics of individual patients, thereby improving treatment outcomes and quality of life for those affected by CRPC.

#### 3.4 The OSAR Validation Results

The high coefficient of determination (R<sup>2</sup>) of 0.9467 and adjusted R<sup>2</sup> of 0.9461 indicate strong correlations between chemical features and AR1 inhibition, which explains approximately 94.67% of the variance in the dataset. The low Standard Error of Estimation (SEE) and Mean Absolute Error (MAE) reflect minimal prediction error, while the Q<sup>2</sup>(LOO) value of 0.9451 demonstrates its robust predictive performance on unseen data.





Furthermore, the external validation metrics confirm the model's generalizability and reliability when applied to separate test compounds. High values of Q<sup>2</sup> (F1) Test and Q<sup>2</sup> (F2) Test, along with a Concordance Correlation Coefficient (CCC) Test value of 0.9715, indicate strong predictive performance on the test set. The stability of the model across different subsets of the training data is supported by the scaled average Rm<sup>2</sup>(LOO) and scaled delta Rm<sup>2</sup>(LOO) metrics. The validation results confirm the accuracy, precision, and robustness of the QSAR model in predicting AR1 inhibitor activity. This suggests its potential utility in guiding the discovery and development of novel compounds for treating non-metastatic castration-resistant prostate cancer by targeting the AR1 protein.

#### **Internal Validation Metrics:**

\*\*\*\*\*\*\*

 $R^2 = 0.9467$   $R^2(Adjusted) = 0.9461$  Standard Error of Estimation (SEE) = 2.5959  $Q^2(LOO) = 0.9451$  SDEP(LOO) = 2.615  $Scaled average Rm^2(LOO) = 0.9214$   $Scaled delta Rm^2 (LOO) = 0.0461$  Mean Absolute Error (MAE, Model-Predicted) = 1.9209 Mean Absolute Error (MAE, LOO) = 1.9489 Prediction Quality (MAE-based criteria) = GOOD

# External Validation Metrics Using a Test Set:

Number of Test set datapoints: 120 Q^2 (F1) Test = 0.9461 Q^2 (F2) Test = 0.9459 Scaled average Rm^2(Test) = 0.8809 Scaled delta Rm^2 (Test) = 0.0486 CCC (Test) = 0.9715 Mean Absolute Error (MAE, Test) = 2.0086 Prediction Quality (MAE-based criteria, Test) = GOOD

#### 3.5 Standard Precision Docking Results of Top 25 Hits of Extracted Compounds from Zinc Database

Based on Glide standard precision docking, the top 25 compounds exhibited relatively higher Glide GScore and MMGBSA dG Bind values for AR1 protein than the standard in this study, with ZINC78824417 showing the highest binding values (Figure 7). The higher binding values suggest stronger interactions between these compounds and the AR1 protein, thus indicating their potential effectiveness as AR1 inhibitors. The Glide GScore is a scoring system that evaluates the binding affinity of a ligand to its target protein in molecular docking simulations. A higher GScore often indicates better binding interaction, implying greater therapeutic potential. Similarly, the MMGBSA dG Bind value, determined from molecular mechanics/generalized Born surface area calculations, sheds light on the binding free energy of the ligand-protein complex, with larger MMGBSA dG Bind values indicating stronger ligand-protein interaction. Thus, the fact that these top compounds exhibited superior binding values compared to the standard compound is promising, as it suggests their potential as potent AR1 inhibitors. The relatively higher binding affinity implies that these compounds may have a greater ability to disrupt AR1 activity, which is often desirable in the context of diseases such as prostate cancer where AR1 plays a significant role.

#### 3.6 Quantum Polarized Ligand Docking Results of Top 25 Hits of Extracted Compounds from Zinc Database

The top 25 compounds exhibited relatively higher XP GScore and MMGBSA dG Bind values for AR1 protein than the standard in this study, with ZINC92180466 showing the highest binding values (Figure 8). These compounds demonstrated superior binding affinity to the target protein, suggesting their potential as strong inhibitors or modulators of AR activity.



Int. J. Biomed. Health Sci. 2025; 19(1): 61-85

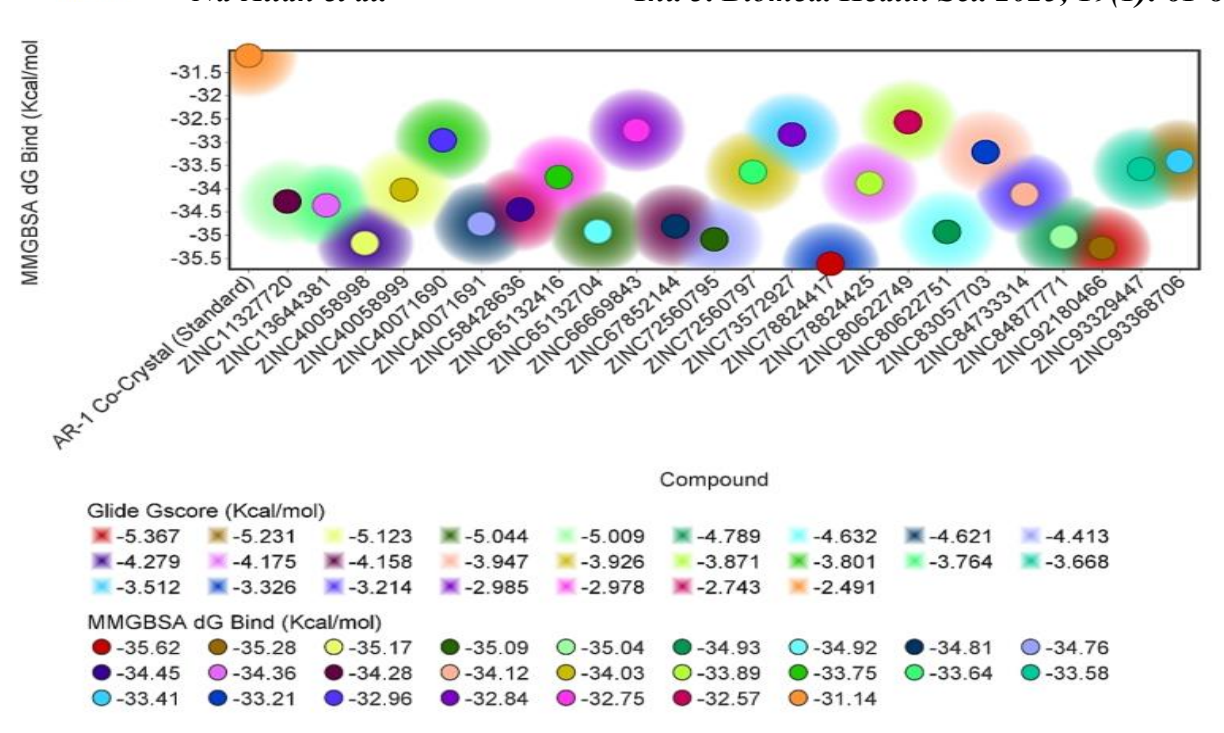


Figure 7: Comparative Glide GScore and MMGBSA dG Bind Values of Top 25 Hits of Extracted Compounds from Zinc Database

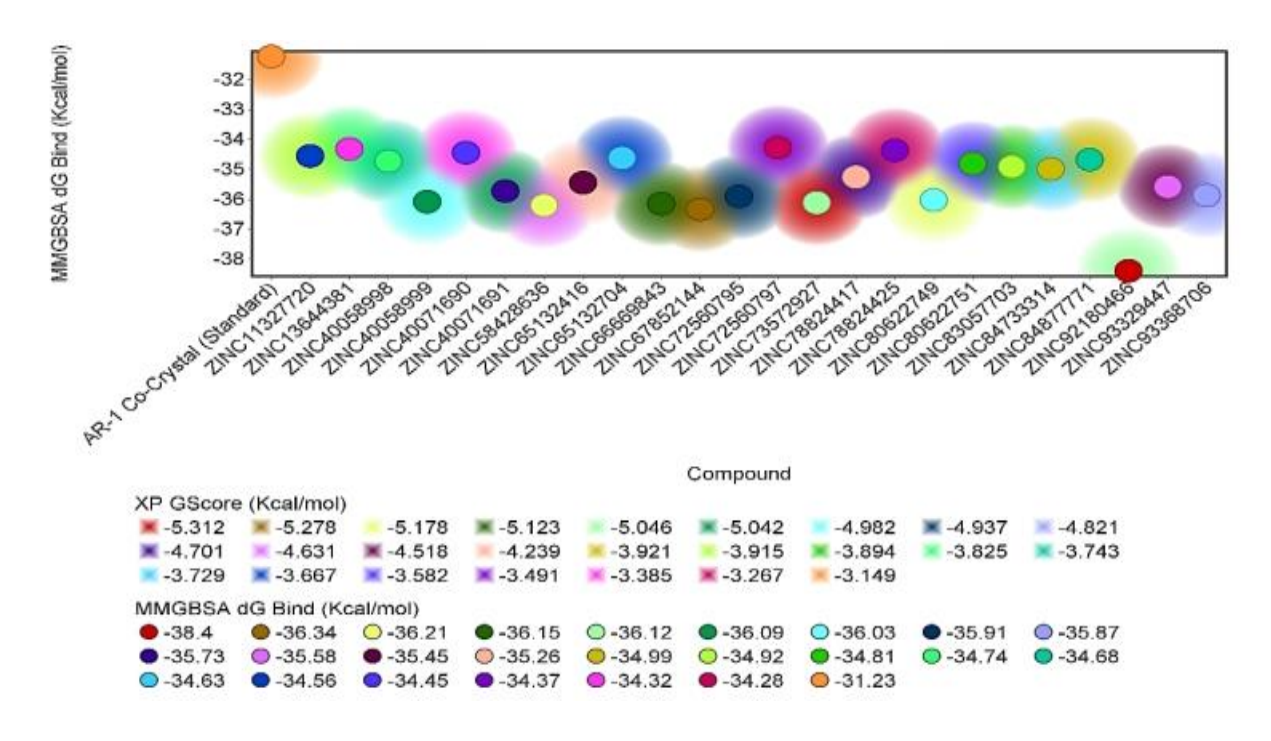


Figure 8: Comparative XP GScore and MMGBSA dG Bind Values of Top 25 Hits of Extracted Compounds from Zinc Database





Among these compounds, ZINC92180466 stood out with the highest binding values, which indicates that it is a particularly promising candidate for further investigation and development. The XP GScore, derived from Glide quantum polarized docking, is a scoring function used to evaluate the binding affinity between a ligand and a protein target. A higher XP GScore value indicates a stronger interaction between the ligand and the receptor, suggesting greater potential for biological activity. Similarly, the MMGBSA dG Bind value, which is calculated by using molecular mechanics generalized Born surface area free energy change, provides insights into the binding energy of the ligand-receptor complex, with compounds exhibiting higher MMGBSA dG Bind values having more favorable binding interactions potential with the protein target.

The significance of these findings lies in identifying compounds with enhanced binding properties compared to the standard compound used in the study. Such compounds hold promises for developing novel therapeutics or chemical probes targeting the AR pathway, which plays a crucial role in various physiological processes and disease states, including prostate cancer. Moreover, the utilization of Glide quantum polarized docking underscores the rigor and reliability of the computational approach employed in this study, by employing advanced molecular docking techniques that can effectively screen large compound libraries and prioritize candidates with the highest likelihood of binding to the target protein with high affinity. Overall, the identification of top-performing compounds with higher binding characteristics for the AR1 protein, particularly ZINC92180466, highlights the potential of computational drug discovery approaches in identifying lead compounds for further experimental validation and development into potential therapeutic agents. These findings contribute to the ongoing efforts aimed at discovering novel treatments for non-metastatic CRPC.

#### 3.7 Induced Fit Docking Results of Top 25 Hits of Extracted Compounds from Zinc Database

The top 25 compounds also demonstrated notably higher induced fit docking (IFD) scores in this study when compared to the standard compound following IFD simulations (Figure 9). These findings indicate that these compounds have a stronger binding affinity towards the target protein, which suggests their potential as effective inhibitors or modulators of the biological activity associated with AR1 protein. IFD simulations enhance the flexibility of both ligands and protein receptors thereby providing a more accurate representation of ligand-receptor interactions in a dynamic environment. The higher IFD score values obtained from these simulations suggest that the top 25 compounds exhibited more optimized binding interactions with the flexible target protein following the induced fit docking process, which further confirms the efficacy potential of these compounds on the AR1 protein. Moreso, ZINC92180466, among the top-performing compounds, stood out with the highest binding values, which indicates its strong potential as a lead candidate for further investigation. The superior binding characteristics of ZINC92180466 following docking simulation, suggest that it possesses desirable pharmacological properties, which render it a promising candidate for drug development efforts targeting non-metastatic CRPC. Furthermore, the use of IFD simulations underscores the sophistication of the computational methods employed in this study. By considering the flexibility of both ligands and the protein receptors, IFD provides a more realistic representation of interactions between the compounds and proteins, thereby enhancing the reliability of the virtual screening process.

# 3.8 Binding Interaction Between Androgen Receptor 1 Protein and the Ligands

The reference (standard) compound binds to Val 730 and Asp 731 of the AR1 protein through the conventional hydrogen bond at average bond distances of 5.34 Å and 4.24 Å respectively, as well as Lys 720, Val 716, and Met 734 of the protein through the hydrophobic alkyl and Pi-alkyl bond at the distances of 5.12 Å, 3.61 Å, and 4.84 Å respectively (Figure 10). This compound is known to modulate the activity of the protein by binding to the binding function 3 (BF3) region of the protein active pocket. Like the standard compound, ZINC92180466 binds to Val 716, Lys 720, and Met 734 of the AR 1 protein through the hydrophobic alkyl and an attractive charge at bond distances of 5.07 Å, 4.62 Å, and 5.28 Å. This is in addition to binding relatively tighter to Gln 738 of the protein through the Pi-Donor hydrogen bond at 2.59 Å, Glu 897 through the conventional hydrogen bond at the distance of 1.88 Å, as well as Met 894 at the bond distance of 5.21 Å (Figure 11). This may have been responsible for the observed relatively higher induced fit docking score of the ZINC92180466 compound than the standard.



This comparison highlights the differences in binding characteristics and effects on AR1 protein activity between the reference compound and the ZINC92180466 compound. The targeted amino acids and the strength of binding interactions contribute to the observed differences in their induced fit docking scores, which indicates potential variations in their efficacy as AR1 protein activity modulators.

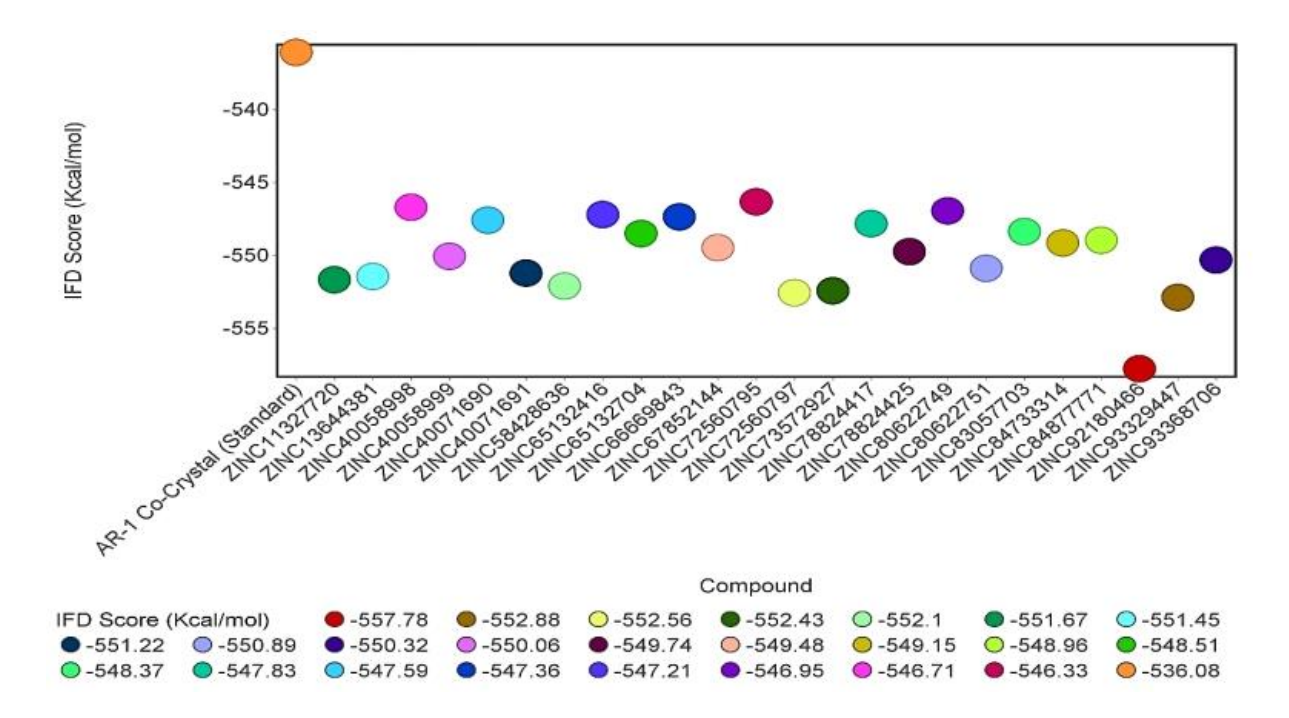


Figure 9: Comparative IFD Score Values of Top 25 Hits of Extracted Compounds from Zinc Database

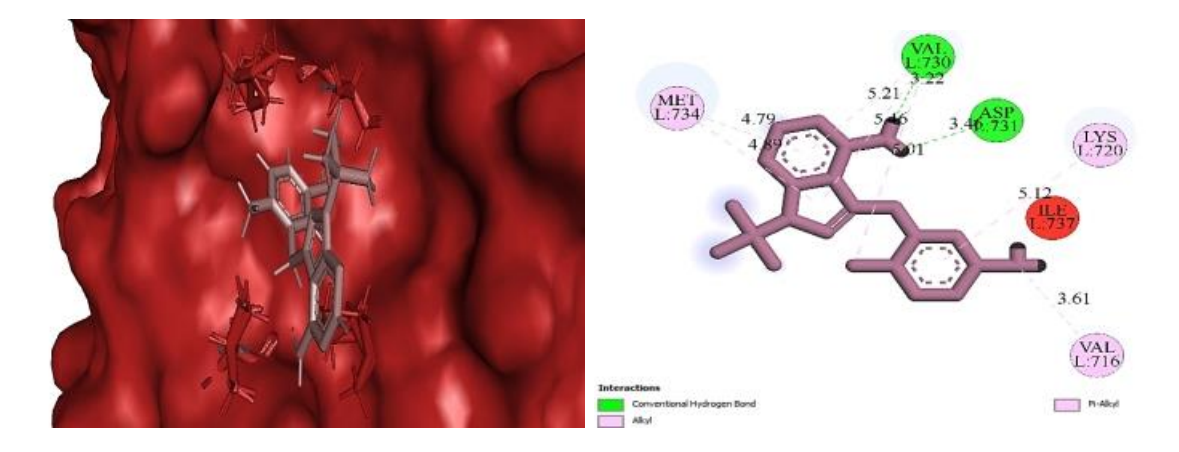


Figure 10: Comparative pocket view and 2D structure of ligand-protein interactions between the standard compound and AR1 protein



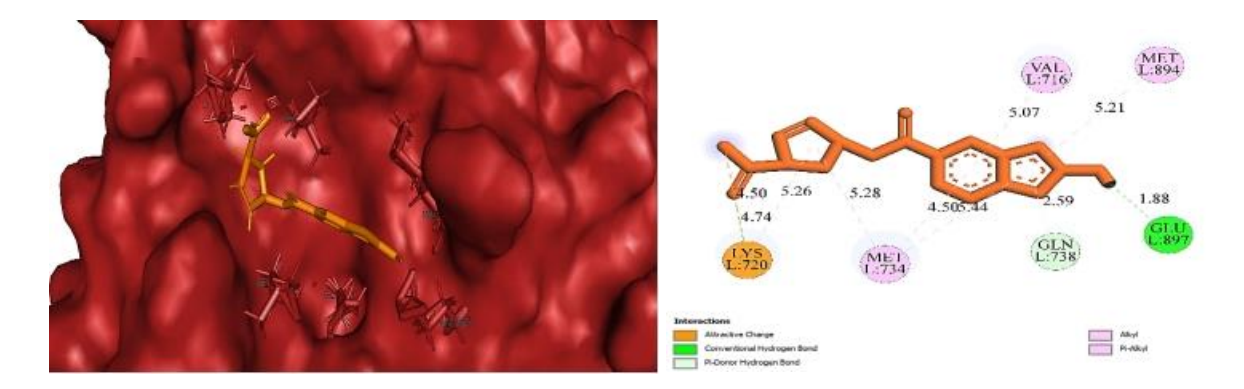


Figure 11: Comparative pocket view and 2D structure of ligand-protein interactions between ZINC92180466 and AR1 Protein

3.9 Molecular Dynamics Simulation of Complexes Between ZINC92180466 and the Protein Co-Crystal

Table 1 presents the averages and standard deviations of all the studied parameters (RMSD, RMSF, RoG, SASA, and number of H-bonds) while Figures 12-16 show the spectral plots obtained for co-crystal\_complex and ZINC92180466\_complex during 100 ns molecular dynamics simulation (MDS). RMSD plots are used to examine the protein stability of the system since they display the degree of each frame's divergence from the original structure [61]. Following an approximate 10-ns equilibration phase for the RMSD plots for both complexes, the simulation proceeded with little fluctuation that was in the acceptable range for the course of the simulation (Figure 12). The ZINC92180466\_complex presented the maximum fluctuation around 45 ns after which the simulation continued with minimal fluctuation until the end. Both the spectral plots and computed mean RMSD show that the binding of the docked compounds did not distort the structural integrity of the protein targets. The RMSF plots demonstrate the flexibility of various enzyme regions. Both complexes showed little fluctuation for the duration of the simulation in the RMSF charts (Figure 13). Both complexes also presented similar mean RMSF values (Table 1). The internal flexibility of the protein was not distorted by the binding of the compounds [62].

The examination of the RoG plots allowed for additional measurement of the bound systems' compactness. Typically, the solvent accessible surface area (SASA) plots show the quantity of solvent accessible by the protein surface. Both RoG and SASA determine the integrity of the folded protein especially during ligand binding. Moreover, the RoG plots of the system were equilibrated before 10 ns and continued throughout the simulation (Figure 14). The two complexes presented similar mean SASA values, and the spectral plots showed minimal fluctuation (Figure 15). Findings from this study showed that the integrity of the folded protein was not distorted by the binding of the ligands, hence the compactness of the protein structures was not compromised [63,64]. Throughout the simulation, there were not many changes in the number of H-bonds. The complexes showed a close mean number of hydrogen bonds (Figure 16).

Table 1: Parameters Analyzed from MDS Trajectories of Docked Compounds Complexed with Target Protein

	RMSD (Å)	RMSF (Å)	RoG (Å)	SASA (Å)	H-Bonds (Å)
Co-crystal_Complex	$1.63\pm0.25$	$0.73\pm0.33$	$18.48 \pm 0.06$	$13102.9 \pm 210.71$	$62.77 \pm 6.49$
ZINC92180466_Complex	$1.86 \pm 0.25$	$0.79 \pm 0.36$	$18.54 \pm 0.06$	$13263.0 \pm 193.72$	$60.55\pm6.45$

Values are expressed as Mean ± Standard Deviation



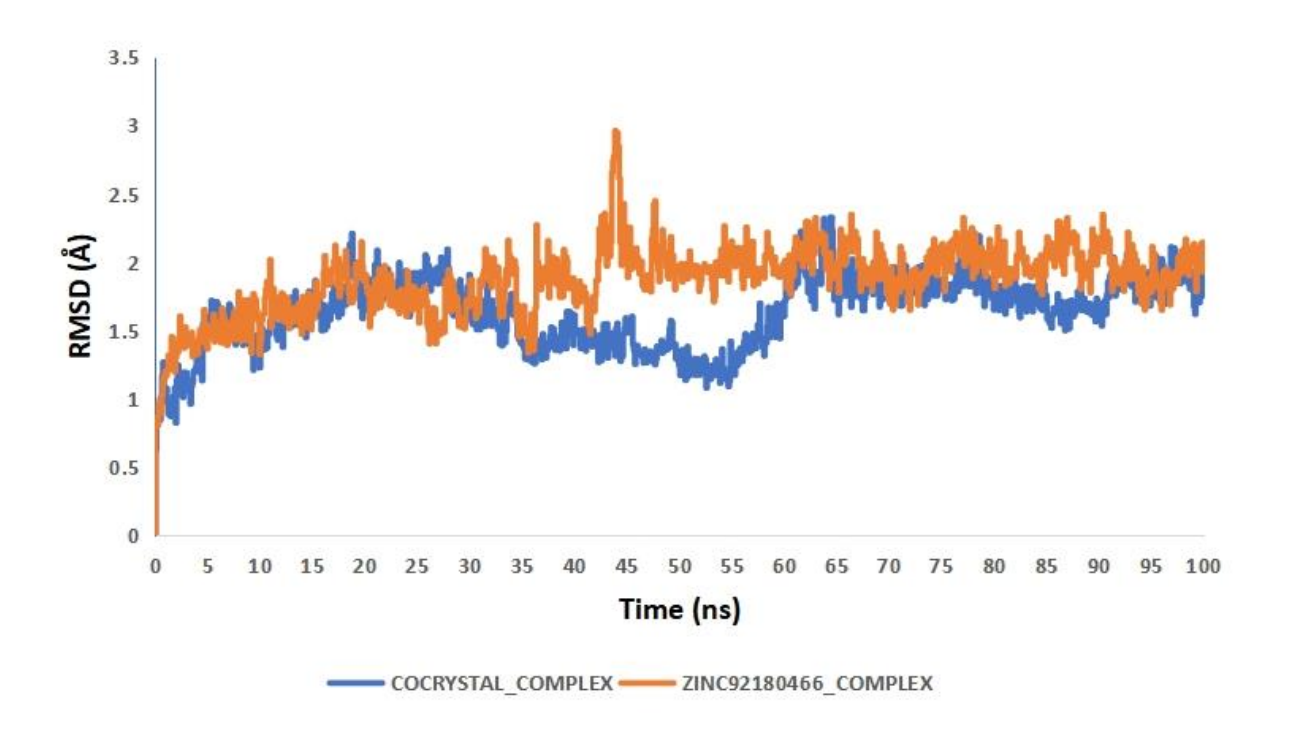


Figure 12: RMSD plots of MDS of docked compound complexed to the target protein

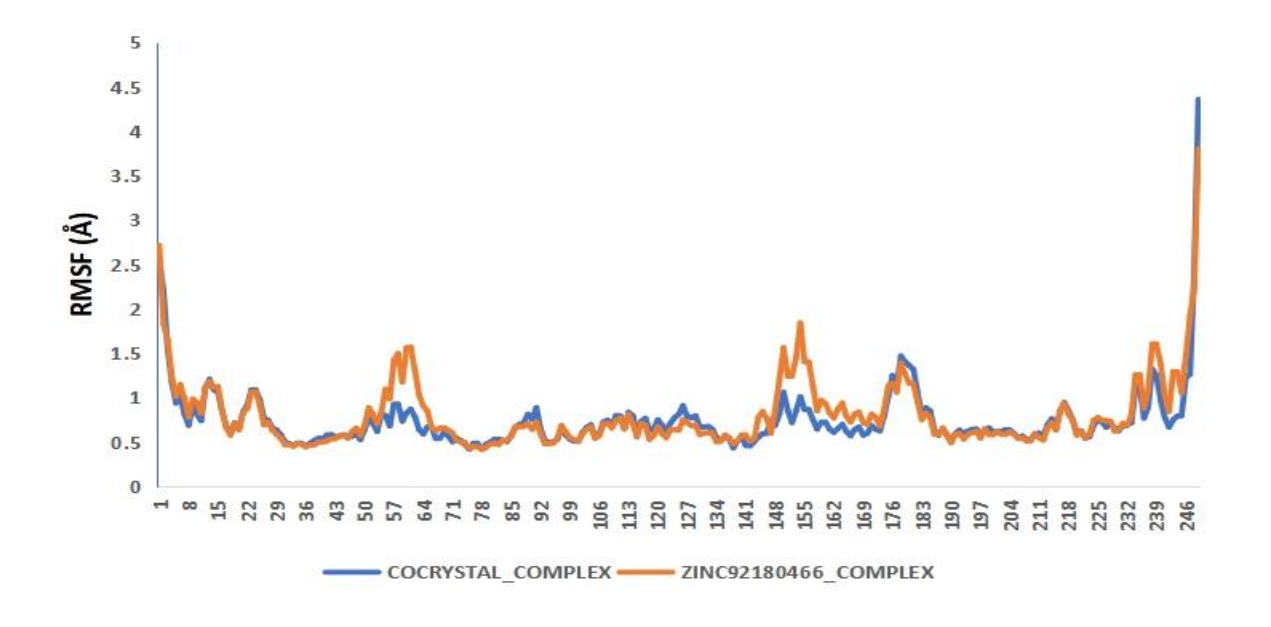


Figure 13: RMSF plots of MDS of docked compound complexed to the target protein



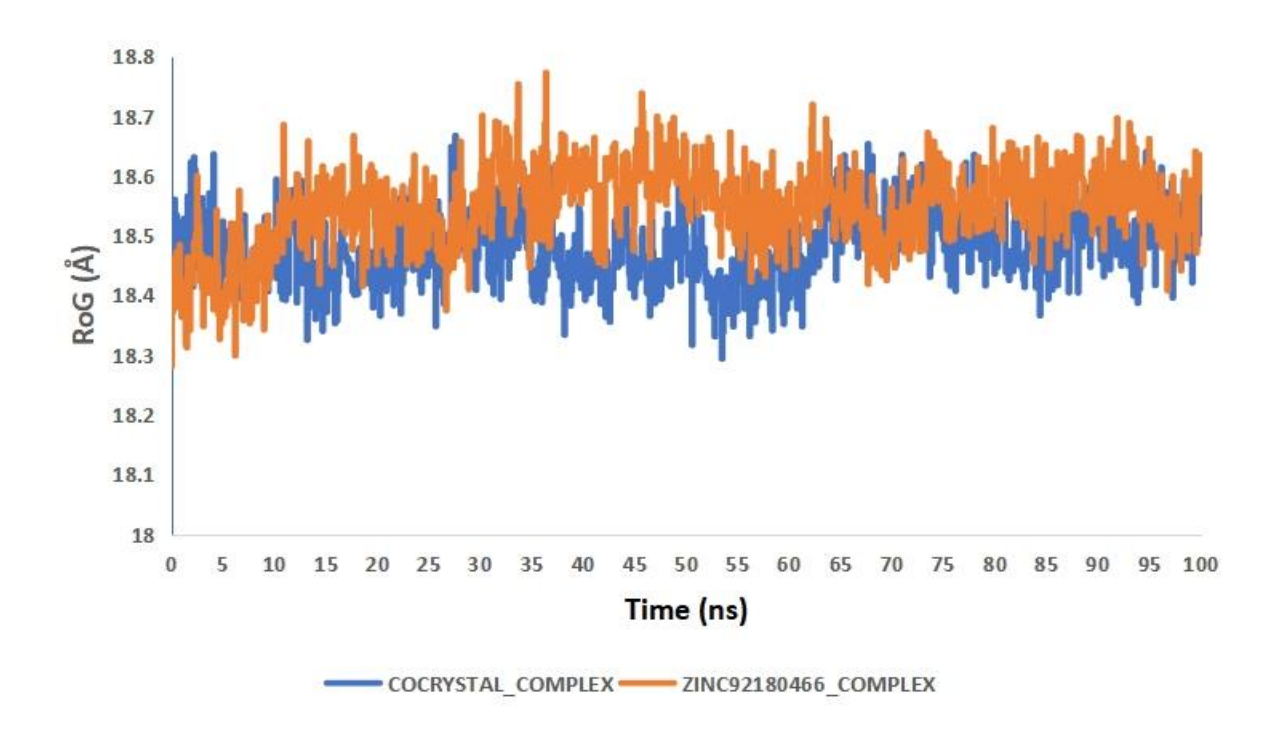


Figure 14: RoG plots of MDS of docked compound complexed to the target protein

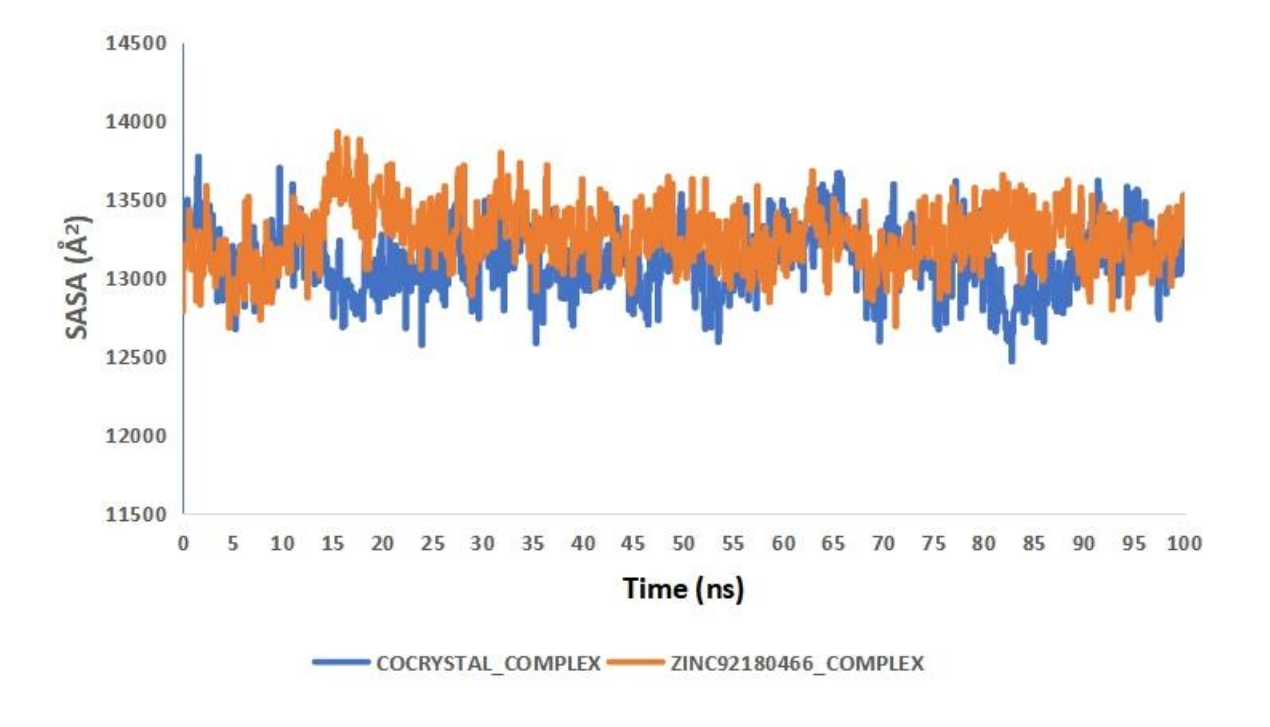


Figure 15: SASA plots of MDS of docked compound complexed to the target protein



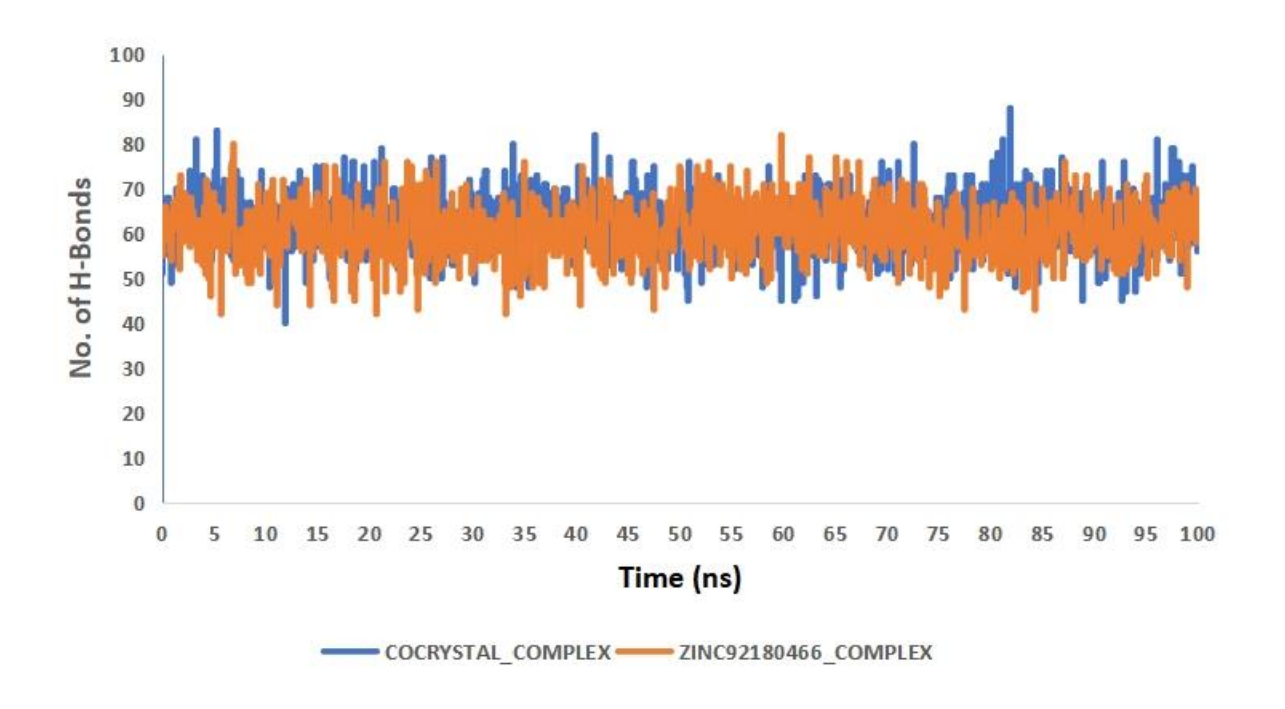


Figure 16: Plots showing changes in the number of H-bonds during MDS of docked compound complexed to the target protein

#### 3.10 Molecular Mechanics Generalized Born Surface Area (MMGBSA) Analysis

From the computed binding free energy, ZINC92180466 demonstrated lower binding free energy (-17.21  $\pm$  3.96) when compared to co-crystal compound (-14.12  $\pm$  8.73). The result from the binding free energy computation in a dynamic mode corroborated the static docking analysis. Table 2 lists the several components that add up to the overall binding free energy. Simulation-based quantitative estimates of the free binding affinity energy of ligands to proteins have been demonstrated to be more precise and dependable in a dynamic context [65]. Using decomposition analysis, the contributing amino acids that make up the overall binding energy were determined. It was observed that the interacting residues during the static docking were majorly involved in the contribution to the total binding free energy. For the co-crystal\_complex, the amino acid residue that contributed more than -1 kcal/mol include Val716, Met734, and Met894 (Figure 17), while those involved in the ZINC92180466\_complex include Lys720, Arg726, Met734, and Met894 that are known to be present in the binding function 3 (BF3) region of the AR1 protein active pocket (Figure 18).

Table 2: Different components energy involved in the binding free energy of docked to target proteins

SYSTEM	$\Delta_{ m VDWAALS}$	$\Delta_{ m EEL}$	$\Delta_{\mathrm{EGB}}$	$\Delta_{\mathrm{ESURF}}$	$\Delta_{ m GGAS}$	$\Delta_{ m GSOLV}$	$\Delta_{ ext{TOTAL}}$
COCRYSTAL_COMPLEX	-14.21 ± 8.70	-153.8 ± 65.7	$156.6 \pm 62.0$	-2.78 ± 1.36	$-168.0 \pm 68.5$	$153.9 \pm 61.0$	$-14.12 \pm 8.73$
ZINC92180466_COMPLEX	-24.45 ± 4.22	-3.15 ± 7.17	$13.80 \pm 7.21$	-3.41 ± 0.60	$-27.60 \pm 8.84$	$10.39 \pm 6.93$	$-17.21 \pm 3.96$

Values are expressed as Mean  $\pm$  Standard Deviation



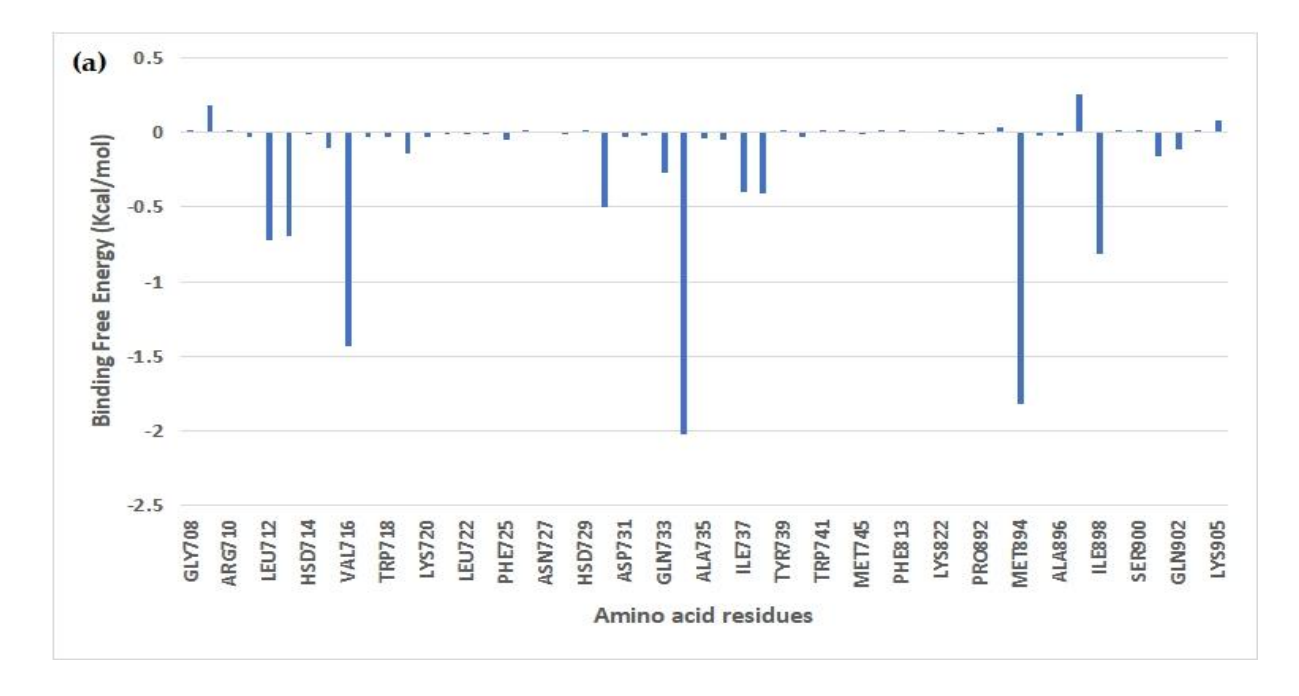


Figure 17: MMPBSA free energy decomposition of residues within 10Å of target protein Complexed with Cocrystal ligand

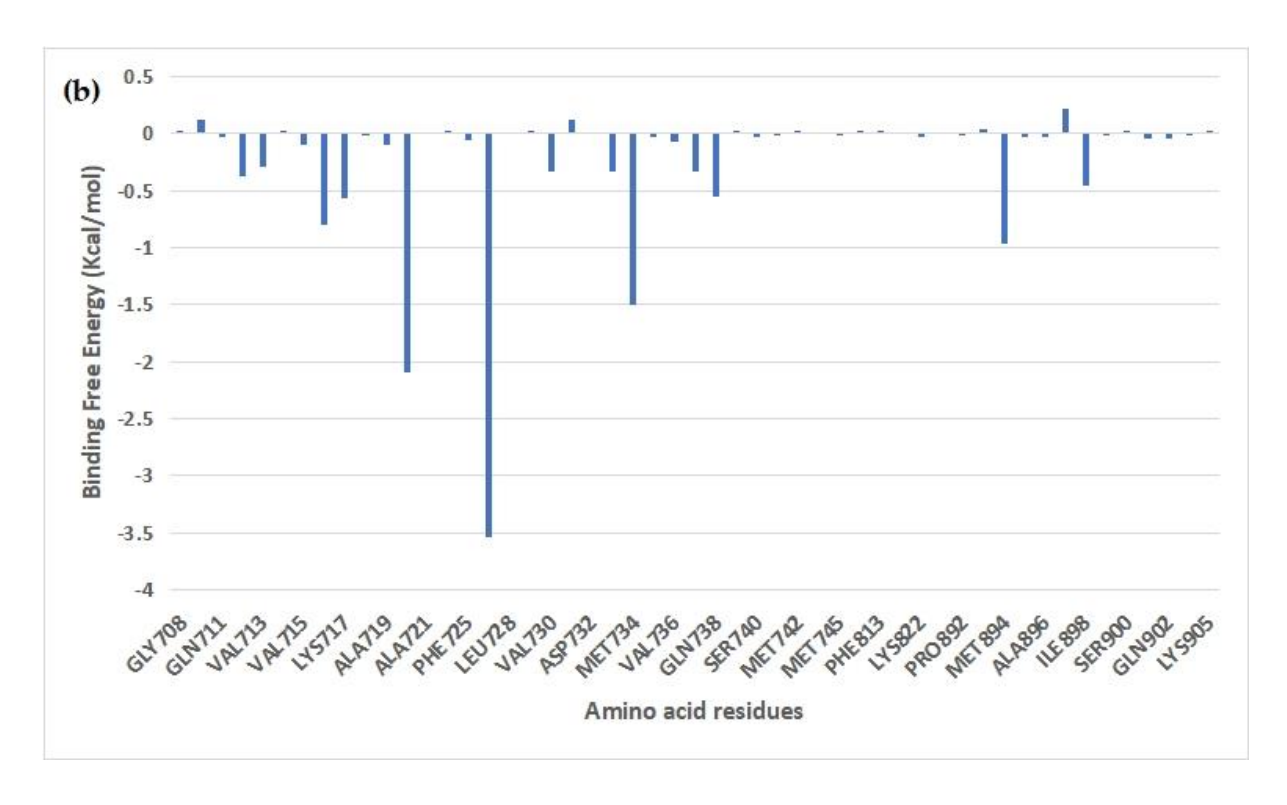


Figure 18: MMPBSA free energy decomposition of residues within  $10\mbox{\normalfont\AA}$  of target protein Complexed with ZINC92180466



#### 4.0 Conclusion

The results of the comprehensive ligand-based pharmacophore modeling of five androgen receptor 1 (AR1) inhibitors provide valuable insights into the structural requirements for effective AR1 inhibition and the identification of common pharmacophoric features, including hydrogen bond donors, acceptors, aromatic rings, and hydrophobic groups, underscores the critical regions being responsible for their inhibitory potency.

The generated pharmacophore model yielded consensus hypotheses with the best model (based on the highest hyposcore), representing the optimal arrangement of pharmacophoric features for AR1 inhibition. This hypothesis offers a structural framework for the rational design of novel AR1 inhibitors to guide chemical modifications for the enhancement of therapeutic potential of the compound against AR1 protein, with profound implications for the development of optimized non-metastatic castration-resistant prostate cancer therapeutics, while the analysis of induced fit docking and molecular dynamics simulations of binding of purchasable compounds extracted from the ZINC database based on this model reveals ZINC92180466 as the compound with the highest resultant binding free energy and stability metrics without significantly distorting the structural integrity of AR1 protein, thus suggesting the suitability of this compound for further investigation and development. Furthermore, its decomposition analysis identified key amino acid residues contributing to the overall binding energy, thereby providing insights into the molecular interactions driving this ligand-receptor binding.

Therefore, in conclusion, the continuous exploration of AR-targeted therapies, especially those focusing on non-LBD sites like BF3, offers promising avenues in combating castration-resistant prostate cancer. With the AR1 protein playing a pivotal role in disease progression and resistance mechanisms of non-metastatic castration-resistant prostate cancer, novel small molecule ARBF-3 binder such as ZINC92180466 identified in this study through advanced computational techniques hold potential for enhanced therapeutic strategies against the disease to ultimately improve patient survival and quality of life.

#### **Funding**

This research was funded by Tertiary Education Trust Fund (TETFUND), Nigeria, through Institutional-Based Research, KWASUIBR/CRIT/070422/VOL2/TETF2021/0017.

#### Acknowledgement

We extend our sincere gratitude to Kwara State University, Malete, Nigeria, for generously providing all the essential facilities crucial for conducting this research. Their support has been invaluable in facilitating our study and advancing our scientific endeavors.

#### **Conflict of Interest**

The authors declare that they have no known competing financial interests or personal relationships that could have appeared to influence the work reported in this paper.

#### References

- [1] Goebell, P.J., Raina, R., Chen, S., Rege, S., Shah, R., Grossman, J.P. and Waldeck, A.R. (2024) Real-world treatment of metastatic hormone-sensitive prostate cancer in the USA, Europe and Asia. Future Oncology, Vol. 20, No. 14, pp. 903–918. https://doi.org/10.2217/fon-2023-0814
- [2] Armstrong, A.J., Szmulewitz, R.Z., Petrylak, D.P., Holzbeierlein, J., Villers, A., Azad, A. et al. (2019). A randomized, phase III study of androgen deprivation therapy with enzalutamide or placebo in men with metastatic hormone-sensitive prostate cancer. Journal of Clinical Oncology, Vol. 37, pp. 2974–2986. https://doi.org/10.1200/JCO.19.00799.
- [3] Mitsogianni, M., Papatsoris, A., Bala, V.M., Issa, H., Moussa, M. and Mitsogiannis, I. (2023). An overview of hormonal directed pharmacotherapy for the treatment of prostate cancer. Expert Opinion in Pharmacotheraphy, Vol, 7, pp. 1–10. https://doi.org/10.1080/14656566.2023.2244415





- [4] Beretta, G.L. and Zaffaroni, N. (2019). Androgen receptor-directed molecular conjugates for targeting prostate cancer. Frontier in Chemistry, Vol 7, pp. 369. <a href="https://doi.org/10.3389/fchem.2019.00369">https://doi.org/10.3389/fchem.2019.00369</a>.
- [5] Schmidt, K.T., Huitema, A.D., Chau, C.H. and Figg, W. D. (2021). Resistance to second-generation androgen receptor antagonists in prostate cancer. Nature Reviews Urology, Vol 18, pp 209–226. <a href="https://doi.org/10.1038/s41585-021-00438-4">https://doi.org/10.1038/s41585-021-00438-4</a>.
- [6] Hussain, M., Fizazi, K., Shore, N.D., Heidegger, I., Smith, M.R., Tombal, B. and Saad, F. (2024). Metastatic Hormone-Sensitive Prostate Cancer and Combination Treatment Outcomes: A Review. JAMA Oncology, Vol. 10, No. 6, pp. 807–820. <a href="https://doi:10.1001/jamaoncol.2024.0591">https://doi:10.1001/jamaoncol.2024.0591</a>.
- [7] Chi, K.N., Agarwal, N., Bjartell, A., Chung, B.H., Gomes, A.J. P. D.S., Given, R., et al. [2019]. Apalutamide for metastatic, castration-sensitive prostate cancer. New England Journal of Medicine, Vol. 381, pp. 13–24. <a href="https://doi.org/10.1056/NEJMoa1903307">https://doi.org/10.1056/NEJMoa1903307</a>.
- [8] Saad, F., Sternberg, C.N., Efstathiou, E., Fizazi, K., Modelska, K., Lin, X., et al. (2020). Prostate-specific antigen progression in enzalutamide-treated men with non-metastatic castration-resistant prostate cancer: Any rise in prostate-specific antigen may require closer monitoring. European Urology, Vol. 78, pp. 847-853. <a href="https://doi.org/10.1016/j.eururo.2020.08.025">https://doi.org/10.1016/j.eururo.2020.08.025</a>.
- [9] Chung, B.H., Horie, S. and Chiong, E. (2020). Clinical studies investigating the use of leuprorelin for prostate cancer in Asia. Prostate International, Vol, 8, pp. 1–9. doi: 10.1016/j.prnil.2019.06.001.
- [10] Fu, W., Yang, H., Hu, C., Liao, J., Gong, Z., Zhang, M., et al. (2023). Small-molecule inhibition of androgen receptor dimerization as a strategy against prostate cancer. ACS Central Science, Vol. 9, pp. 675–684. doi: 10.1021/acscentsci.2c01548.
- [11] Sahai, E., Astsaturov, I., Cukierman, E., DeNardo, D.G., Egeblad, M., Evans, R.M. et al. (2020). A framework for advancing our understanding of cancer-associated fibroblasts. Nature Review Cancer, Vol. 20, pp. 174–186. https://doi.org/10.1038/s41568-019-0238-1.
- [12] Clarke, N.W., Armstrong, A.J., Thiery-Vuillemin, A., Oya, M., Shore, N., Loredo, E. et al. (2022). Abiraterone and olaparib for metastatic castration-resistant prostate cancer. New England Journal of Medicine Evidence, Vol. 1(9), EVIDoa2200043. <a href="https://doi.org/10.1056/EVIDoa2200043">https://doi.org/10.1056/EVIDoa2200043</a>.
- Davis, I.D., Martin, A.J., Stockler, M.R., Begbie, S., Chi, K.N., Chowdhury, S. et al. Enzalutamide with standard first-line therapy in metastatic prostate cancer. New England Journal of Medicine, Vol. 381, pp. 121–131. https://doi.org/10.1056/NEJMoa1903835.
- [14] Harris, A.E., Metzler, V.M., Lothion-Roy, J., Varun, D., Woodcock, C.L., Haigh, D.B. et al. (2022). Exploring antiandrogen therapies in hormone-dependent prostate cancer and new therapeutic routes for castration-resistant prostate cancer. Frontier in Endocrinology, Vol. pp. 13. Article 1006101. <a href="https://doi.org/10.3389/fendo.2022.1006101">https://doi.org/10.3389/fendo.2022.1006101</a>.
- [15] Mehralivand, S., Thomas, C., Puhr, M., Claessens, F., van de Merbel, A.F., Dubrovska, A. et al. (2024). New advances of the androgen receptor in prostate cancer: report from the 1st International Androgen Receptor Symposium. Journal of Translational Medicine, Vol. 22, pp. 71. https://doi.org/10.1186/s12967-024-04878-5
- [16] Gustafson, J.L., Neklesa, T.K., Cox, C.S., Roth, A.G., Buckley, D.L., Tae, H.S. et al. (2015). Small-molecule-mediated degradation of the androgen receptor through hydrophobic tagging. Angewandte Chemie International Edition, Vol. 54, pp. 9659–9662. https://doi.org/10.1002/anie.201503720.



- [17] Kregel, S., Wang, C., Han, X., Xiao, L., Fernandez-Salas, E., Bawa, P., et al. (2020). Androgen receptor degraders overcome common resistance mechanisms developed during prostate cancer treatment. Neoplasia, Vol. 22, pp. 111–119. https://doi.org/10.1016/j.neo.2019.12.003.
- [18] Han, X., Wang, C., Qin, C., Xiang, W., Fernandez-Salas, E., Yang, C.Y., et al. (2019). Discovery of ARD-69 as a highly potent proteolysis targeting chimera (PROTAC) degrader of androgen receptor (AR) for the treatment of prostate cancer. Journal of Medical Chemistry, Vol. 62, No. 2, pp. 941–964. <a href="https://doi.org/10.1021/acs.jmedchem.8b01631">https://doi.org/10.1021/acs.jmedchem.8b01631</a>.
- [19] Hussain, M., Mateo, J., Fizazi, K., Saad, F., Shore, N., Sandhu, S., Chi, K.N., et al. (2020). Survival with olaparib in metastatic castration-resistant prostate cancer. New England Journal of Medicine, Vol. 383, No. 24, pp. 2345–2357. https://doi.org/10.1056/NEJMoa2022485.
- [20] He, Y., Hwang, D.J., Ponnusamy, S., Thiyagarajan, T., Mohler, M.L., Narayanan, R., et al. (202). Pyrazol-1-yl-propanamides as SARD and pan-antagonists for the treatment of enzalutamide-resistant prostate cancer. Journal of Medical Chemistry, Vol. 63, No. 21, pp. 12642–12665. https://doi.org/10.1021/acs.jmedchem.0c00943.
- [21] Han, X., Zhao, L., Xiang, W., Qin, C., Miao, B., McEachern, D. et al. (2021). Strategies toward discovery of potent and orally bioavailable proteolysis targeting chimera degraders of androgen receptor for the treatment of prostate cancer. Journal of Medicinal Chemistry, Vol. 6, No. 17, pp. 12831–12854. <a href="https://doi.org/10.1021/acs.jmedchem.1c00882">https://doi.org/10.1021/acs.jmedchem.1c00882</a>.
- [22] Isaacs, J.T. (2018). Resolving the Coffey paradox: What does the androgen receptor do in normal vs. malignant prostate epithelial cells? American Journal of Clinical and Experimental Urology, Vol. 6, No. 2, pp. 55–61. PMCID: PMC5902723/PMID: 29666833.
- [23] Kanayama, M., Lu, C., Luo, J. and Antonarakis, E.S. (2021). AR splicing variants and resistance to AR targeting agents. Cancers (Basel), Vol. 13, pp. 2563. https://doi.org/10.3390/cancers13112563.
- Zhang, D. Zhao, S., Li, X., Kirk, J.S. and Tang, D.G. (2018). Prostate luminal progenitor cells in development and cancer. Trends in Cancer, Vol. 4, pp. 769–783. https://doi.org/10.1016/j.trecan.2018.09.003.
- [25] Li, D., Zhou, W., Pang, J., Tang, Q., Zhong, B., Shen, C., et al. (2021). A magic drug target: Androgen receptor. Medicinal Research Reviews, Vol. 39, No. 5, pp. 1485–1514. https://doi.org/10.1002/med.21558.
- [26] Labrecque, M.P., Alumkal, J.J., Coleman, I.M., Nelson, P.S. and Morrissey, C. (2021). The heterogeneity of prostate cancers lacking AR activity will require diverse treatment approaches. Endocrine-Related Cancer, Vol. 28, No. 8, pp. T51–T66. https://doi.org/10.1530/ERC-21-0002.
- [27] Rani, A., Dasgupta, P. and Murphy, J.J. (2019). Prostate Cancer: The Role of Inflammation and Chemokines. American Journal of Pathology, Vol. 189, pp. 2119–2137. https://doi.org/10.1016/j.ajpath.2019.07.007.
- [28] Van Poppel, H. and Abrahamsson, P. A. (2020). Considerations for the use of gonadotropin-releasing hormone agonists and antagonists in patients with prostate cancer. International Journal of Urology, Vol. 27, No. 10, pp. 830–837. <a href="https://doi.org/10.1111/iju.14303">https://doi.org/10.1111/iju.14303</a>.
- [29] Shen, G., Chen, J., Zhou, Y., Wang, Z., Ma, Z. and Xu, C. (2018). Azd5153 inhibits prostate cancer cell growth in vitro and in vivo. Cellular Physiology and Biochemistry, Vol. 50, pp. 798–809. https://doi.org/10.1159/000494244.
- [30] Menges, D., Yebyo, H.G., Sivec-Muniz, S., Haile, S.R., Barbier, M.C.;,Tomonaga, Y. et al. (2020). Treatments for metastatic hormone-sensitive prostate cancer: Systematic review, network meta-analysis, and benefitharm assessment. European Urology Oncology, Vol. 5, No. 6, pp. 605–616. <a href="https://doi.org/10.1016/j.euo.2022.04.007">https://doi.org/10.1016/j.euo.2022.04.007</a>.



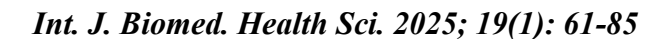


- [31] McAllister, M.J., Underwood, M.A., Leung, H.Y. and Edwards, J. (2019). A review on the interactions between the tumor microenvironment and androgen receptor signaling in prostate cancer. Translational Research, Vol. 206, pp. 91–106. https://doi.org/10.1016/j.trsl.2018.11.004.
- [32] Small, E.J., Saad, F., Chowdhury, S., Oudard, S., Hadaschik, B.A., Graff, J.N., et al. (2020). Final survival results from SPARTAN, a phase III study of apalutamide (APA) versus placebo (PBO) in patients (pts) with nonmetastatic castration-resistant prostate cancer (nmCRPC). Journal of Clinical Oncology, Vol. 38, pp. 5516. https://doi.org/10.1200/JCO.2020.38.15 suppl.5516.
- [33] Pagliuca, M., Buonerba, C., Fizazi, K. and Di Lorenzo, G. (2019). The Evolving Systemic Treatment Landscape for Patients with Advanced Prostate Cancer. Drugs, Vol. 79, No. 4, pp. 381–400. <a href="https://doi.org/10.1007/s40265-019-1060-5">https://doi.org/10.1007/s40265-019-1060-5</a>.
- [34] Siegel, R. L., Miller, K.D. and Jemal, A. (202). Cancer statistics, 2020. CA: Cancer Journal of Clinicians, Vol. 70, pp. 7–30. <a href="https://doi.org/10.3322/caac.21590">https://doi.org/10.3322/caac.21590</a>.
- [35] Tucci, M., Caffo, O., Buttigliero, C., Cavaliere, C., D'Aniello, C., Di Maio, M., Kinspergher, S. et al. (2019). Therapeutic options for first-line metastatic castration-resistant prostate cancer: Suggestions for clinical practice in the CHAARTED and LATITUDE era. Cancer Treatment Reviews, Vol. 74, pp. 35–42. <a href="https://doi.org/10.1016/j.ctrv.2019.01.002">https://doi.org/10.1016/j.ctrv.2019.01.002</a>.
- [36] Ng, K., Smith, S. and Shamash, J. (2020). Metastatic hormone-sensitive prostate cancer (mHSPC): advances and treatment strategies in the first-line setting. Oncology Therapy, Vol. 8, pp. 209–230. https://doi.org/10.1007/s40487-020-00119-z.
- [37] Estebanez-Perpina, E., Bevan, C.L. and McEwan, I.J. (2021). Eighty years of targeting androgen receptor activity in prostate cancer: The fight goes on. Cancers (Basel), Vol. 13, No. 3, pp. 509–527. <a href="https://doi.org/10.3390/cancers13030509">https://doi.org/10.3390/cancers13030509</a>.
- [38] Fei, J., Zhou, L., Liu, T. and Tang, X.Y. (2013). Pharmacophore Modeling, Virtual Screening, and Molecular Docking Studies for Discovery of Novel Akt2 Inhibitors. International Journal of Medical Science, Vol. 10, No. 3, pp. 265-275. https://doi.org/10.7150/ijms.5344.
- [39] Delhommelle, J. (2011). Recent Advances in Molecular Simulation. Molecular Simulation, Vol. 37, No. 7, pp. 515-515. <a href="https://doi.org/10.35248/ijirset.22.3(5).55-60">https://doi.org/10.35248/ijirset.22.3(5).55-60</a>.
- [40] Agu, P.C., Afiukwa, C.A., Orji, O.U., Ezeh, E.M., Ofoke, I.H., Ogbu, C.O., et al. (2023). Molecular docking as a tool for the discovery of molecular targets of nutraceuticals in diseases management. Scientific Reports, Vol. 13, pp. 13398. https://doi.org/10.1038/s41598-023-40160-2.
- [41] Beavers, M.P., Myers, M.C., Shah, P.P., Purvis, J.E., Diamond, S.L., Cooperman, B.S., et al. (2008). Molecular Docking of Cathepsin L Inhibitors in the Binding Site of Papain. Journal of Chemical Information and Modelling, 48(7): 1464–1472. <a href="https://doi.org/10.1021/ci800085c">https://doi.org/10.1021/ci800085c</a>
- [42] Chauhan, K. and Kumar, K. (2022). Molecular Docking of Medicinal Plant Compounds as New Potential Inhibitors of Novel Coronavirus. International Journal of Innovative Research in Science, Engineering and Technology, 3 (5): 055-060. <a href="https://doi.org/10.35248/ijirset.22.3(5).55-60">https://doi.org/10.35248/ijirset.22.3(5).55-60</a>.
- [43] Mateev, E., Georgieva, M. and Zlatkov, A. (2023). Improved Molecular Docking of MAO-B Inhibitors with Glide. Biointerface Research in Applied Chemistry, Vol. 13, No. 2, pp. 159. <a href="https://doi.org/10.33263/BRIAC132.159">https://doi.org/10.33263/BRIAC132.159</a>.
- [44] Huang, S.Y. and Zou, X. (2010). Advances and Challenges in Protein-Ligand Docking. International Journal of Molecular Sciences, Vol. 11, No. 8, pp. 3016-3034. https://doi.org/10.3390/ijms11083016.





- [45] Chen, Y.C. (2015). Beware of docking! Trends in Pharmacological Sciences, Vol. 36, No. 2, pp. 1-14. https://doi.org/10.1016/j.tips.2014.12.001.
- [46] Thirunavukkarasu, M.K. and Karuppasamy, R. (2022). Drug Repurposing Combined with MM/PBSA-based Validation Strategies Towards MEK Inhibitors Screening. Journal of Biomolecular Structure and Dynamics, Vol. 40, No. 22, pp. 12392-12403. https://doi.org/10.1080/07391102.2021.1970629.
- [47] Nada, H., Lee, K., Gotina, L., Pae, A.N. and Elkamhawy, A. (2022). Identification of novel discoidin domain receptor 1 (DDR1) inhibitors using E-pharmacophore modeling, structure-based virtual screening, molecular dynamics simulation and MM-GBSA approaches. Computers in Biology and Medicine, pp. 142, <a href="https://doi.org/10.1016/j.compbiomed.2022.105217">https://doi.org/10.1016/j.compbiomed.2022.105217</a>.
- [48] Gyebi, G.A., Ogunyemi, O.M., Ibrahim, IM., Afolabi, S.O. and Adebayo, J.O. (2021). Dual targeting of cytokine storm and viral replication in COVID-19 by plant-derived steroidal pregnanes: An *in silico* perspective. Computers in Biology and Medicine, pp. 134 104406. doi:10.1016/j.compbiomed.2021.104406
- [49] Ogunyemi, O.M., Gyebi, G.A., Ibrahim, I.M., Olaiya, C.O., Ocheje, J.O., Fabusiwa, M.M. et al. (2021). Dietary stigmastane-type saponins as promising dual-target directed inhibitors of SARS-CoV-2 proteases: a structure-based screening. RSC Advance, Vol. 11, No. 53, pp. 33380-33398. https://doi.org/10.1039/d1ra05976a.
- [50] Ojo, A.B., Gyebi, G.A., Alabi, O., Iyobhebhe, M., Kayode, A.B., Nwonuma, C.O. et al. (2022a). Syzygium aromaticum (L.) merr. & LM perry mitigates iron-mediated oxidative brain injury via in vitro, ex vivo, and in silico approaches. Journal of Molecular Structure, Vol. 1268, pp. 133675. <a href="https://doi.org/i10.1016/j.molstruc.2022.133675">https://doi.org/i10.1016/j.molstruc.2022.133675</a>.
- [51] Brooks, B.R., Brooks, C.L., Mackerell, A.D., Jr., Nilsson, L., Petrella, R.J., Roux, B. et al. (2009). CHARMM: the biomolecular simulation program. Journal in Computational Chemistry, Vol. 30, No. 10, pp.1545-614. https://doi.org/10.1002/jcc.21287.
- [52] Jo, S., Cheng, X., Islam, S.M., Huang, L., Rui, H., Zhu, A. et al. (2014). CHARMM-GUI PDB manipulator for advanced modeling and simulations of proteins containing nonstandard residues. Advances I Protein Chemistry and Structural Biology, Vol. 96, pp. 235-265. https://doi.org/10.1016/bs.apcsb.2014.06.002.
- [53] Jo, S., Kim, T.I., yer Vidyashankara, G. and Charmm-gui, W.I. (2008). A web-based graphical user interface for CHARMM SUNHWAN. Journal in Computational Chemistry, Vol. 29, pp. 1859-1865. <a href="https://doi.org/10.1002/jcc.20945">https://doi.org/10.1002/jcc.20945</a>.
- [54] Abraham, M.J., Murtola, T., Schulz, R., Páll, S., Smith, J.C., Hess, B. et al. (2015). GROMACS: High performance molecular simulations through multi-level parallelism from laptops to supercomputers. SoftwareX, Vol. 1, pp. 19-25. https://doi.org/10.1016/j.softx.2015.06.001.
- [55] Govindarajan, N., Tiwari, A., Ensing, B. and Meijer, E.J. (2018). Impact of the ligand flexibility and solvent on the O–O bond formation step in a highly active ruthenium water oxidation catalyst. Inorganic Chemistry, Vol. 57, No. 21, pp. 13063-13066. <a href="https://doi.org/10.1021/acs.inorgchem.8b00619">https://doi.org/10.1021/acs.inorgchem.8b00619</a>.
- [56] Hess, B., Bekker, H., Berendsen, H.J. and Fraaije, J.G. (1997). LINCS: A linear constraint solver for molecular simulations. Journal in Computational Chemistry, Vol. 18, No. 12, pp.1463-1472. doi.org/10.1002/(SICI)1096987X(199709)18:12%3C1463::AIDJCC4%3E3.0.CO;2-H
- [57] Essmann, U., Perera, L., Berkowitz, M.L., Darden, T., Lee, H. and Pedersen, L.G. (1995). A smooth particle mesh Ewald method. Journal of Chemical Physics, Vol. 103, No. 19, pp. 8577-8593. <a href="https://doi.org/10.1063/1.470143">https://doi.org/10.1063/1.470143</a>.





- [58] Valdés-Tresanco, M.S., Valdés-Tresanco, M.E., Valiente, P.A. and Moreno, E. (2021). gmx\_MMPBSA: a new tool to perform end-state free energy calculations with GROMACS. Journal of Chemical Theory and Computation, Vol. 17, No. 10, pp. 6281-6291. https://doi.org/10.1063/1.470117.
- [59] Miller III B.R., McGee Jr, T.D., Swails, J.M., Homeyer, N., Gohlke, H. and Roitberg, A.E. (2012). MMPBSA. py: an efficient program for end-state free energy calculations. Journal of Chemical Theory and Computation, Vol. 8, No. 9, pp. 3314-3321. doi: 10.1021/ct300418h.
- [60] Ojo, O.A., Ogunlakin, A.D., Iyobhebhe, M., Olowosoke, C.B., Taiwo, O.A., Akinola, A., et al. (2022b). Computer aided and experimental study of cinnamic acid analog for oxidative stress treatment: The therapeutic validations. Informatics in Medicine Unlocked, Vol. 35, pp. 101137. https://doi.org/10.1016/j.imu.2022.101137.
- [61] Cheng, X. and Ivanov, I. (2012). Molecular dynamics. Methods in Molecular Biology, Vol.1, pp. 243-285. https://doi.org/10.1007/978-1-62703-050-2 11.
- [62] Dong, Y.W., Liao, M., Meng, X. and Somero, G.N. (2018). Structural flexibility and protein adaptation to temperature: Molecular dynamics analysis of malate dehydrogenases of marine molluscs. Proceedings of the National Academy of Science, Vol. 115, No. 6, pp. 1274-1279. <a href="https://doi.org/10.1073/pnas.1718910115">https://doi.org/10.1073/pnas.1718910115</a>.
- [63] Sinha, S. and Wang, S.M. (2020). Classification of VUS and unclassified variants in BRCA1 BRCT repeats by molecular dynamics simulation. Computational and Structural Biotechnology Journal, Vol. 18, pp. 723-736. <a href="https://doi.org/10.1016/j.csbj.2020.03.013">https://doi.org/10.1016/j.csbj.2020.03.013</a>.
- [64] Okoli, B.J., Eltayb, W.A., Gyebi, G.A., Ghanam, A.R., Ladan, Z., Oguegbulu, J.C., et al. (2022). In Silico Study and Excito-Repellent Activity of Vitex negundo L. Essential Oil against Anopheles gambiae. Applied Sciences, Vol. 12, No. 15, pp. 7500. <a href="https://doi.org/10.3390/app1215750">https://doi.org/10.3390/app1215750</a>.
- [65] Perez, A., Morrone, J.A., Simmerling, C. and Dill, K.A. (2016). Advances in free-energy-based simulations of protein folding and ligand binding. Current Opinion in Structural Biology, Vol. 36, pp. 25-31. <a href="https://doi.org/10.1016/j.sbi.2015.12.002">https://doi.org/10.1016/j.sbi.2015.12.002</a>.